

Chemo-spectrophotometric evolution of spiral galaxies:

I. The model and the Milky Way

S. Boissier and N. Prantzos

Institut d'Astrophysique de Paris, 98bis, Bd. Arago, 75104 Paris

ABSTRACT

The chemical and spectro-photometric evolution of spiral galaxies is investigated with detailed models, making use of up-to-date ingredients (like metallicity dependent stellar properties) and a prescription for the star formation rate (SFR) justified both empirically and theoretically. As a first application, the model is used to describe the evolution of the Milky Way. The role of the adopted scheme of disk formation (“inside-out”) in shaping the various chemical and colour profiles is investigated, as well as the role of extinction. It is shown that the solar neighborhood does not evolve as the Milky Way as a whole and that one-zone models with a non-linear SFR prescription cannot be used to study the evolution of our Galaxy. Our model average SFR is shown to match well observations of external spirals.

Key words: Galaxy: evolution - Galaxy: general - Galaxy: structure - galaxies: evolution - galaxies: spiral - galaxies: photometry

1 INTRODUCTION

Galactic evolution is one of the major topics of research in modern astrophysics. Despite more than three decades of intense observational and theoretical studies, the subject has not yet reached the maturity of other fields, like e.g. stellar evolution. Our limited understanding of the “driver” of galactic evolution i.e. star formation from the interstellar medium, is the main reason for this situation.

Galactic disks are privileged places for the study of the star formation rate (SFR) since their various properties (surface densities of stars and gas, SFR, abundances of various elements, luminosity and colour profiles etc.) can be measured as a function of galactocentric distance and compared to theoretical predictions. Notice that predictions for the SFR exist only for disk galaxies (based on various instability criteria, e.g. Talbot and Arnett 1975, Onihishi 1975, Wyse and Silk 1989, Dopita and Ryder 1994), not for ellipticals or irregulars. Testing these predictions against the largest observational data set is obviously crucial for our understanding of the SFR.

Until recently, detailed observed properties of disk galaxies were available only for the local universe, i.e. at very low redshift. These data offer information only about the current status of galaxies, from which their past history is to be derived; in view of the many model parameters, it is difficult to deduce a unique history from those data (in one single case, namely the Milky Way, we have information on the local disk history, via the age-metallicity relationship and the metallicity distribution of low mass stars). The spectacular progress in instrumentation makes now possible the

observation of galaxy morphology at higher redshifts (e.g. Lilly et al. 1998) and will soon allow to compare models to observations covering the largest part of galaxy evolution.

The various aspects of galactic evolution, namely dynamical, chemical and spectro-photometric, have usually been treated separately up to now (with a few exceptions). A large number of multi-zone chemical evolution models have been proposed, matching in a relatively satisfactory way the current chemical properties of the Milky Way disk (e.g. Matteucci and François 1989, Ferrini et al. 1994, Prantzos and Aubert 1995, Carigi 1996, Tosi 1998, Dwek 1998) or the (much less constraining) chemical profiles of external spirals (e.g. Molla et al. 1997); in some cases, this class of models takes into account the possibility of radial flows of gas in the galactic disks (e.g. Mayor and Vigroux 1981, Lacey and Fall 1985, Clarke 1989, Tsujimoto et al. 1995, Firmani et al. 1996). On the other hand, one-zone spectrophotometric evolution models (treating the whole galaxy as one single region) have been developed, matching the integrated photometric properties of spirals along the Hubble sequence (usually varying the SFR time-scale, e.g. Guiderdoni and Rocca-Volmerange 1987, Bruzual and Charlot 1993, Arimoto et al. 1992); these models do not provide a detailed study of the chemical properties or of the photometric gradients in spirals. Preliminary multi-zone chemo-photometric evolution models have been studied by Talbott and Arnett (1975), while more recent ones were applied to low surface brightness galaxies (e.g. Jimenez et al. 1998).

Chemo-dynamical evolution models have been developed and applied to spirals by a few groups (Steinmetz and

Muller 1994; Theis et al. 1997); these models have a less sophisticated treatment of chemical evolution than the classical ones and are still subject to the uncertainties of initial conditions and gas-stars interactions. In a recent work, Conrardo et al. (1998) made the first attempt, to our knowledge, to combine in a single computation photometry, chemistry and dynamics; despite the failure to reproduce basic observational properties of the Milky Way disk (like the local G-dwarf metallicity distribution - see Sec. 3.1.1 - or colour gradients at low redshifts) this type of model seems quite promising and shows the way that galactic evolution studies should take in the future; however, in view of the large and many uncertainties affecting dynamical models (and their coupling to chemistry) at present, the way towards a convincing unified treatment is expected to be rather long.

This paper is the first of a series aiming to study in a unified framework the chemical *and* spectrophotometric properties of spiral galaxies, with appropriate detailed multi-zone models. Here we present in some detail the model and its application to the Milky Way, which will serve as “template” for further studies. In Sec. 2.1 we present the chemical evolution part of the model, justifying our choice of the adopted SFR law (Sec. 2.1.2) In Sec. 2.2 we present the spectro-photometric part of the model, emphasizing the homogeneity of the adopted sets of stellar tracks and spectra (both as a function of metallicity) and the importance of a correct treatment of metallicity-dependent stellar lifetimes in the calculation of the photometric evolution. In Sec. 3.1 we present the results of the model for the chemical and photometric evolution of the solar neighborhood and study the effects of metallicity-dependent ingredients and of extinction on those results. In Sec. 3.2 we present the results for the Milky Way disk and we discuss the evolution of the various chemical and photometric gradients and the (limited) role of extinction in shaping the latter; we also discuss the populations of stellar remnants and their role on various aspects of studies of the Galaxy. In Sec. 3.3 we compare the evolution of the solar neighborhood to the one of the Milky Way as a whole and show that they differ considerably, i.e. one-zone models reproducing the local disk properties cannot be used to simulate the evolution of the whole Galaxy. In Sec. 3.4 we compare (favourably) the average SFR of the model with recent observations of the corresponding SFR in external spirals (from Kennicutt 1998). Finally, our main results are summarized in Sec. 4.

2 THE MODEL

2.1 Chemical evolution

The adopted model of galactic chemical evolution has been presented in previous works (i.e. Prantzos and Aubert 1995, hereafter PA95; Prantzos and Silk 1998, hereafter PS98). The classical set of the equations of galactic chemical evolution (Tinsley 1980; Pagel 1997) is solved numerically for each zone, without the Instantaneous Recycling Approximation. Instantaneous mixing is assumed within each zone, i.e. at the star’s death its ejecta are thoroughly mixed in the local interstellar medium, which is characterized by a unique composition at any time (no abundance scatter is obtained in that framework). The main input physics of the model are described below.

2.1.1 Stellar inputs: yields, remnant masses, lifetimes

The yields of massive stars (i.e. the amount of stellar ejecta in the form of various elements) adopted in this work are those of Woosley and Weaver (1995, hereafter WW95) for metallicity $Z = Z_{\odot}$. Notice that in some cases they differ considerably from the corresponding ones of the other major recent work in the field (Thielemann et al. 1996). These differences are due to the different physical inputs utilised by the two groups, mainly the criterion for convection, the nuclear reaction rates and the determination of the “mass-cut” (see Prantzos 1998b for a review of the role of the yields of massive stars in chemical evolution). The most significant difference concerns the yields of Fe: in the case of WW95 they are increasing with stellar mass, while all massive stars eject $\sim 0.07 M_{\odot}$ of Fe in the case of Thielemann et al. (1996).

For the masses of the stellar remnants we have adopted the following prescriptions. Stars with mass $M < 9 M_{\odot}$ become white dwarfs with mass $M_R(M/M_{\odot}) = 0.1 M/M_{\odot} + 0.45$ (Iben and Tutukov 1984). Stars with $M > 8 M_{\odot}$ explode as accretion induced collapse (in the 8-11 M_{\odot} range) or Fe core collapse (for $M > 11 M_{\odot}$) supernovae, leaving behind a neutron star of mass $M_R = 1.4 M_{\odot}$ (as suggested by observations of neutron stars in binary systems, e.g. Thorsett and Chakrabarty 1998); the heaviest of those stars may form a black hole but the mass limit for its formation is not known at present and cannot be inferred from theoretical or observational arguments (e.g. Prantzos 1994, Bethe and Brown 1995), despite occasional claims for the contrary. Fortunately, due to the steeply decreasing stellar Initial Mass Function in the range of massive stars (see Sec. 2.1.2), the mass limit for stellar black hole formation does not significantly affect the results of chemical evolution, at least as far as that limit is above $\sim 40 M_{\odot}$. Attempts to determine the number and masses of galactic neutron stars and black holes based on the energetics of the supernova explosion and the Fe core mass has been made in Timmes et al. (1996) and Bethe and Brown (1998); we feel however, that the current understanding of these topics does not allow an accurate determination of those parameters and we adopt the aforementioned simple prescription, i.e. stars with $M > 8 M_{\odot}$ leave a neutron star of $1.4 M_{\odot}$, while stars of $M > 40 M_{\odot}$ leave a black hole of $3 M_{\odot}$ (obviously, the adopted values in the case of the black hole formation are lower limits and they serve only for illustration purposes).

There are equally important uncertainties in the yields of $M < 9 M_{\odot}$ stars, due to the treatment of mass loss, envelope convection, etc. especially in their final evolution on the Asymptotic Giant Branch (AGB; see Charbonnel 1998 for a recent review). In this work we have adopted those of Marigo et al. (1996) in the range 1-4 M_{\odot} and those of Renzini and Voli (1981) in the 4-9 M_{\odot} range (their Table 4d with Hot Bottom burning); despite the different physical inputs, the two sets of yields merge rather smoothly in the intermediate mass regime ($\sim 4 M_{\odot}$). In any case, the uncertainties in those yields play a very limited role in the context of this work.

Finally, the adopted stellar lifetimes τ_M as a function of the stellar mass M are from the work of the Geneva group (Schaller et al. 1992, Charbonnel et al. 1996). dependence of the stellar lifetimes (see Fig. 3) may affect considerably the results of photometric evolution (see Sec. 3.1.2).

2.1.2 Stellar Initial Mass Function (IMF)

The choice of the IMF plays a crucial role in the results of chemical and photometric evolution of galaxies. Most photometric studies still use a Salpeter power-law IMF $\Phi(M) \propto M^{-(1+X)}$ with $X=1.35$ in the whole stellar mass range, although Salpeter (1955) derived that IMF in the 0.6-10 M_{\odot} range. However, several studies have shown that the IMF flattens below $M \sim 1 M_{\odot}$ (e.g. Reid and Gizis 1997 and references therein) and the use of a Salpeter IMF over the whole mass range (i.e. down to the H-burning limit) is in disagreement with observational evidence.

Although the flattening of the IMF below $\sim 1 M_{\odot}$ is generally accepted now (e.g. Scalo 1998), its exact shape is still under debate. For instance, Reid and Gizis (1997), using a new sample of M-dwarfs and an up-to-date mass-luminosity calibration, find that a single slope $X=0.05$ can fit the whole mass range $0.1 < M/M_{\odot} < 1$. In a recent review, Kroupa (1998), after discussing all recent determinations of the low mass part of the IMF, favours a slope $X=0.5$ for $M < 0.5 M_{\odot}$ and down to the H-burning limit.

On the other hand, the slope of the high mass part of the IMF is also uncertain. Studies of OB associations on the SMC, LMC and the Milky Way (Massey et al. 1995) show relatively flat slopes ($X \sim 1-1.5$). However, a surprisingly large number of massive stars ($\sim 50\%$) are found outside OB associations according to Massey (1998), who finds that these “field” stars have much steeper IMFs ($X \sim 3-4$ in the Milky Way, LMC and SMC). The slope of $X=1.7$ suggested in Scalo (1986) seems a reasonable choice, on the basis of all available observational data (see Gilmore et al. 1998 and references therein).

The mass limits of the IMF play also an important role in the outcome of galactic evolution studies, in view of the normalisation

$$\int_{M_{min}}^{M_{max}} \Phi(M) M dM = 1 \quad (1)$$

M_{max} is usually taken to be in the 50-100 M_{\odot} range and its exact value affects slightly the results of chemical evolution. The adopted M_{min} is usually $\sim 0.1 M_{\odot}$ (i.e. close to the H-burning limit of $0.08 M_{\odot}$) but lower values cannot be excluded provided they do not violate observational constraints. In the case of the solar neighborhood, one such constraint is that the current surface density of brown dwarfs should not exceed $\sim 8 M_{\odot} \text{ pc}^{-2}$ (Mera et al. 1998), i.e. $\sim 15\%$ of the local surface density. A very small amount of brown dwarfs is also suggested by Reid and Gizis (1997) who find that their IMF drops below $\sim 0.1 M_{\odot}$.

These considerations suggest that there is some freedom in the choice of the IMF. In our recent works (PA95, PS98) we adopted the IMF from the work of Kroupa et al. (1993, hereafter KTG93), where the complex interdependence of several factors (like stellar binarity, ages and metallicities, as well as mass-luminosity and colour-magnitude relationships) is explicitly taken into account. It is a three-slope power-law IMF; in the high mass regime it has a relatively steep slope of $X=1.7$ (based on Scalo 1986), while it flattens in the low-mass range ($X=1.2$ for $0.5 < M/M_{\odot} < 1$, and $X=0.3$ for $M < 0.5 M_{\odot}$). We adopt here again the KTG93 IMF between 0.1 and 100 M_{\odot} , although we are aware that there is some debate as to the exact form of the low-mass

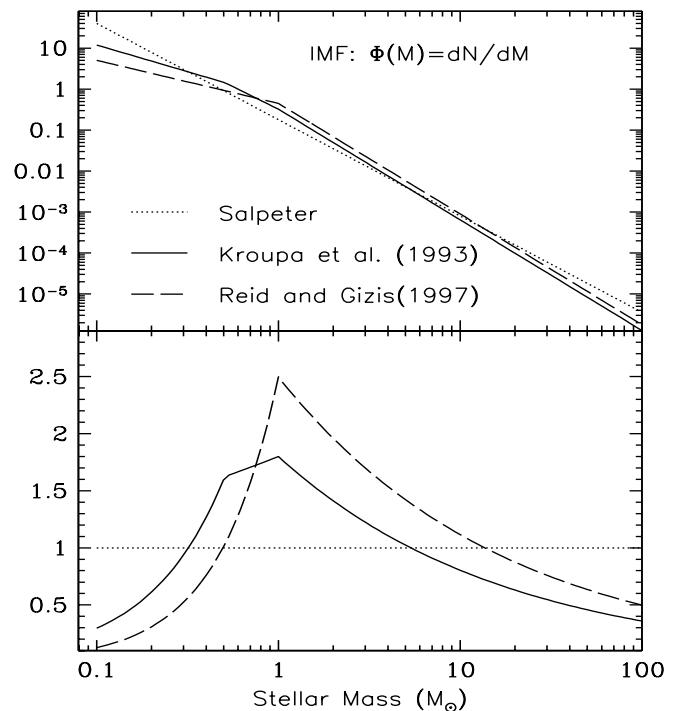


Figure 1. *Upper panel:* Initial mass functions (IMF), according to Salpeter (1955, *dotted* curve with a unique slope $X=1.35$), Reid and Gizis (1997, *dashed* curve) and Kroupa et al. (1993, *solid* curve); the latter is adopted in this work. All curves are normalised according to Equ. 1 (see text). *Lower panel:* ratio of the multi-slope IMFs to the Salpeter IMF; because of the normalisation, they contain more intermediate and low-mass stars and a smaller number of red dwarfs and massive stars.

part (in view of the results of Gould et al. 1997 and Reid and Gizis 1997; see, however, Haywood 1994). The KTG93 IMF is plotted in Fig. 1, where it is compared to the Salpeter IMF and the Reid and Gizis (1997) IMF. The KTG93 IMF has a smaller number of massive stars than the Salpeter IMF and therefore it produces less metals and SNII (although the return mass fraction is similar in the two case: ~ 0.30); on the other hand, it contains a larger number of intermediate and \sim solar mass stars and thus produces more light than the Salpeter IMF (since it is precisely the long-lived 1-2 M_{\odot} stars that contribute most of the galactic light at late times). Notice that the IMF suggested by Reid and Gizis (1997, with $X=0.05$ for $M < 1 M_{\odot}$ and $X=1.7$ for $M > 1 M_{\odot}$) would produce even more light (when appropriately normalised, as in Equ. 1). These considerations have important implications for the chemo-spectrophotometric evolution of galaxies, that are rarely considered; in fact, most studies of photometric evolution adopt a Salpeter IMF in the whole mass range, without worrying about local observational evidence or implications for chemical evolution.

Finally, the question of the variation of the IMF in time or space has not received a satisfactory answer for the moment, although most observers tend to favour the “no variation” option. For instance, Massey et al. (1995) find no difference in the IMF of massive stars in OB associations between the SMC, LMC and the Milky Way, despite the factor

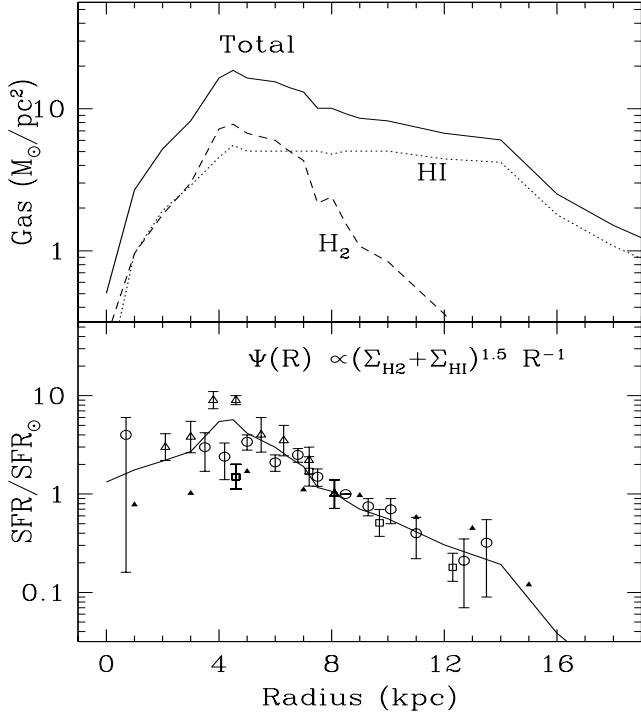


Figure 2. *Upper panel:* Current surface density profiles of molecular (H_2) and atomic (HI) hydrogen in the Milky Way, as a function of galactocentric radius (from Dame 1993) and total gas surface density (the sum of the two, increased by 40% to account for helium). *Lower panel:* Corresponding theoretical current SFR (solid curve, according to Equ. 2) and comparison to observational estimates of the current SFR profile. Data from: Lyne et al. 1985 (open circles), Gusten and Mezger 1983 (triangles), Guibert et al. 1978 (squares). The SFR profiles are normalised to their value at $R_S=8$ kpc.

of ~ 10 difference in metallicity between those regions; also, in a recent work Gizis and Reid (1999) find that the low-mass part of the IMF is the same in local disk and halo stars, i.e. independent of metallicity. On the other hand, Scalo (1998) rejects the “myth of the universality of the IMF”, on the basis of observational and theoretical arguments (for a thorough discussion of all aspects of the IMF see the volume edited by Gilmore et al. 1998).

2.1.3 Star formation rate (SFR)

The adopted star formation rate (SFR) Ψ is locally a Schmidt type law $\Psi \propto \Sigma_G^{1.5}$, where Σ_G is the local gas surface density. Such a proportionality has been suggested by Kennicutt (1989, 1998) on the basis of observations of average SFR vs. gas surface densities in spirals (see Sec. 3.4). On the other hand, a radial dependence of the star formation efficiency in disk galaxies is required in order to reproduce the observed gradients, and such a dependence has indeed been proposed on the basis of various instability criteria for gaseous disks (e.g. Talbot and Arnett 1975; Onihishi 1975; Wyse and Silk 1989; Dopita and Ryder 1994). It should be noted that star formation theories exist and may be tested mainly for disk galaxies, not for e.g. ellipticals or irregulars. We adopt in this

work a star formation rate explicitly dependent on galactocentric radius. It is based on the idea that stars are formed in spiral galaxies when the interstellar medium with angular frequency $\Omega(R)$ is periodically compressed by the passage of the spiral pattern, having a frequency $\Omega_P = \text{const.} < \Omega(R)$. This leads to $\text{SFR} \propto \Omega(R) - \Omega_P \propto \Omega(R)$ and, for disks with flat rotation curves, to $\text{SFR} \propto R^{-1}$ (Wyse and Silk 1989), i.e.

$$\Psi(t, R) = 0.1 \Sigma_G(R)^{1.5} (R/R_S)^{-1} M_\odot \text{pc}^{-2} \text{Gyr}^{-1} \quad (2)$$

where $R_S=8$ kpc is the distance of the Sun to the Galactic centre. Such a radial dependence of the SFR is also compatible with observational evidence, as can be seen in Fig. 2, displaying the current gas surface density profile in the Milky Way disk (upper panel) and the corresponding SFR according to Equ. 2 (lower panel); comparison of this theoretical SFR to observations (lower panel in Fig. 2) shows a fairly good agreement. To our knowledge, this is the first time that this type of direct comparison is pointed out. It has been shown that this form of the SFR can account for the observed gradients of gas fraction, SFR and chemical abundance profiles in the Milky Way (e.g. PS98 and Sec. 3.2.1). One of the major aims of the present work is to derive the corresponding photometric gradients (Sec. 3.2.2) and compare our model average SFR to recent observations concerning external spirals (Sec. 3.4).

2.1.4 Supernova rates

Once the SFR and IMF are fixed, and the lower mass limit M_{SNII} for the formation of Fe core collapse supernova is determined, the corresponding rate of SNII explosions can be calculated as $\text{SNII}(t) = \Psi(t) \int_{M_{\text{SNII}}}^{100 M_\odot} \Phi(M) dM$; we adopt here $M_{\text{SNII}}=8 M_\odot$ (in fact, the most massive of these stars, as well as some of those in close binary systems, will suffer extensive mass losses prior to the explosion and appear as SNIb/c supernovae; but we keep the designation of SNII here for all core collapse events). With the adopted IMF, the integral in the formula above has the value $5.5 \cdot 10^{-3}$, i.e. 0.55 SNII per century are expected for a SFR of $1 M_\odot \text{year}^{-1}$; in the case of a Salpeter IMF, the corresponding number is slightly higher ($7.7 \cdot 10^{-3}$).

On the other hand, a supplementary source of Fe peak nuclei is introduced in the form of type Ia supernovae (SNIa), presumably white dwarfs in binary systems accreting material from their companion star (see Nomoto et al. 1997 for a recent review of SNIa). The relative homogeneity of the observed SNIa lightcurves suggests that $\sim 0.7 M_\odot$ of Fe are ejected (originally in the form of ^{56}Ni); this is also predicted by the most successful models of SNIa, involving carbon deflagration in a Chandrasekhar mass white dwarf. We adopt here the yields of the W7 model from Thielemann et al. (1986). However, the evolution of the SNIa rate in the Galaxy is difficult to predict from the theory of binary systems alone (see e.g. Ruiz-Lapuente et al. 1997 and references therein). We adopt here the prescription of Matteucci and Greggio (1986), in order to reproduce the observed decline of O/Fe vs Fe/H in the local disk. Notice that the recent results of Israelian et al. (1998) and Boesgaard et al. (1999) show a steady decline of that ratio also in halo stars, in disagreement with previous observations showing a “plateau”;

if these new results are confirmed, the SNIa rate formalism should be reconsidered.

The comparison of the model supernova rate (integrated over the disk) to observations of Milky Way type spirals (usually expressed in SNU, i.e. number of supernovae per century and per $10^{10} L_{B,\odot}$) is a crucial test of the model. It is feasible only in the framework of self-consistent models calculating both chemical *and* photometric evolution and has rarely been done up to now (see Sec. 3.3).

2.1.5 Gaseous flows

The disk is assumed to be built by accretion of gas with primordial composition. On purely phenomenological grounds, infall constitutes the most elegant and natural way to account for the G-dwarf problem in the solar neighborhood (e.g. Tinsley 1980, Pagel 1997), but is also supported by some chemodynamical models of the Milky Way (Samland et al. 1997).

The infall rate $f(t, R)$ is normalised to the local disk surface density $\Sigma_T(R)$:

$$\int_0^T f(t, R) dt = \Sigma_T(R) \quad (3)$$

where $T=13.5$ Gyr is the adopted age of the disk. The form of $f(t, R_S = 8 \text{ kpc})$ is adjusted to satisfy the constraint of the G-dwarf metallicity distribution in the solar neighborhood. An exponentially decreasing infall rate $f(t) \propto e^{-t/\tau}$ with $\tau > 7$ Gyr can provide a satisfactory fit to the new data (Chiapini et al. 1997 and Sec. 3.1.1), and we adopt here this minimal value for $\tau(R_S)$. We note that such long time scales for the disc formation (many Gyr) are also obtained in recent chemodynamical models (Samland et al. 1997). To simulate the “inside-out” formation of the disk (suggested by dynamical models, e.g. Larson 1976), the infall timescale $\tau(R)$ is assumed to be radially dependent, taking lower values in the inner regions ($\tau=1$ Gyr at radius $R=2$ kpc) and larger ones in the outer disk ($\tau=10$ Gyr at $R=18$ kpc). The radial variation in the SFR efficiency and in the infall timescale are the only parameters of the model explicitly dependent on radius.

We assume that the disk is evolving as independent one-zone rings. This (over)simplification ignores in general the possibility of radial inflows in gaseous disks, resulting e.g. by viscosity or by infalling gas with specific angular momentum different from the one of the underlying disk; in both cases, the resulting redistribution of angular momentum leads to radial mass flows. The magnitude of the effect is difficult to evaluate, because of our poor understanding of viscosity and our ignorance of the kinematics of the infalling gas. Models with radial inflows have been explored in the past (Mayor and Vigroux 1981; Lacey and Fall 1986; Clarke 1989; Chamcham and Tayler 1994); at the present stage of our knowledge, introduction of radial inflows in the models would imply even more free parameters and make impossible the study of a radial variation in the efficiency of the SFR.

2.2 Spectrophotometric evolution

Once the chemical evolution of a galactic zone has been calculated, its spectro-photometric evolution can be also fol-

wed. The spectrum of the zone at time t is the sum of the individual spectra $l_\lambda(M, t - t', Z(t'))$ of stars of mass M , formed at time $t' < t$ with metallicity $Z(t')$ and still alive at time t :

$$L_\lambda(t) = \int_t \int_M \Psi(t') \Phi(M) l_\lambda(M, t - t', Z(t')) dM dt' \quad (4)$$

This integral can, in principle, be evaluated by integrating first either on time (isomass method) or on mass (isochrone method). The limits of the corresponding integrals are not the same in the two methods. In the first one:

$$L_\lambda(t) = \int_{M_{min}}^{M_{max}} \Phi(M) \left[\int_{t_{inf}(Z(t'))}^t \Psi(t') l_\lambda(M, t - t', Z(t')) dt' \right] dM \quad (4a)$$

while in the second one:

$$L_\lambda(t) = \int_0^t \Psi(t') \left[\int_{M_{min}}^{M_{up}(Z(t'))} \Phi(M) l_\lambda(M, t - t', Z(t')) dM \right] dt' \quad (4b)$$

In the first case (isomass), the lower limit of the first integral (inside []) is $t_{inf}(Z(t')) = t - \tau_M(Z(t'))$ and represents the creation time of the star of mass M dying at time t . This limit depends itself on the integration variable t' of the first integral because of the metallicity dependent lifetimes of stars; obviously, in that case the first integral cannot be calculated and the isomass method cannot be applied. In the second case (isochrone), the upper limit of the first integral (inside []) is $M_{up}(Z(t')) = M[\tau_M(Z(t')) = t - t']$, i.e. it corresponds to the heaviest star created at time t' and dying at time t ; this limit does not depend on the integration variable M and the integration can always be performed. Thus, although the two methods are, in principle, equivalent when metallicity independent lifetimes are considered, *the isochrone method is the only applicable when metallicity dependent lifetimes are taken into account* (as they should). We adopt the second method in this work.

Calculation of the double integral in eqs. (4) requires knowledge of:

a) the stellar IMF $\Phi(M)$; b) the SFR $\Psi(t)$; c) the metallicity $Z(t)$; d) the stellar spectra $l_\lambda(M, t, Z)$ for all evolutionary stages and initial metallicities.

Ingredient (a) is the same as the one adopted in Sec. 2.1.2, ingredients (b) and (c) are obtained self-consistently, by the adopted prescription for the SFR and the run of the chemical evolution model and ingredient (d) is discussed in Sec. 2.2.1 and 2.2.2 below.

Eq. (4b) gives the composite absorption spectrum of the stellar population of the galaxy. This spectrum is subsequently modified by ionisation of the ambient gas (its UV part) and absorption by dust. The (crude) modelisation of the latter process is discussed in Sec. 2.2.3.

2.2.1 Stellar evolution tracks

We adopt in this work the tracks of the Geneva group (Schaller et al. 1992; Charbonnel et al. 1996), concerning stars in the mass range $0.8 \leq M/M_\odot \leq 120$ and in the metallicity range $Z_1=0.05 Z_\odot$ to $Z_2=Z_\odot$. The positions of the stars in the HR diagram (effective temperature T_{eff} and bolometric luminosity L) are given, along with the corresponding ages, at equivalent points of the evolution (e.g.

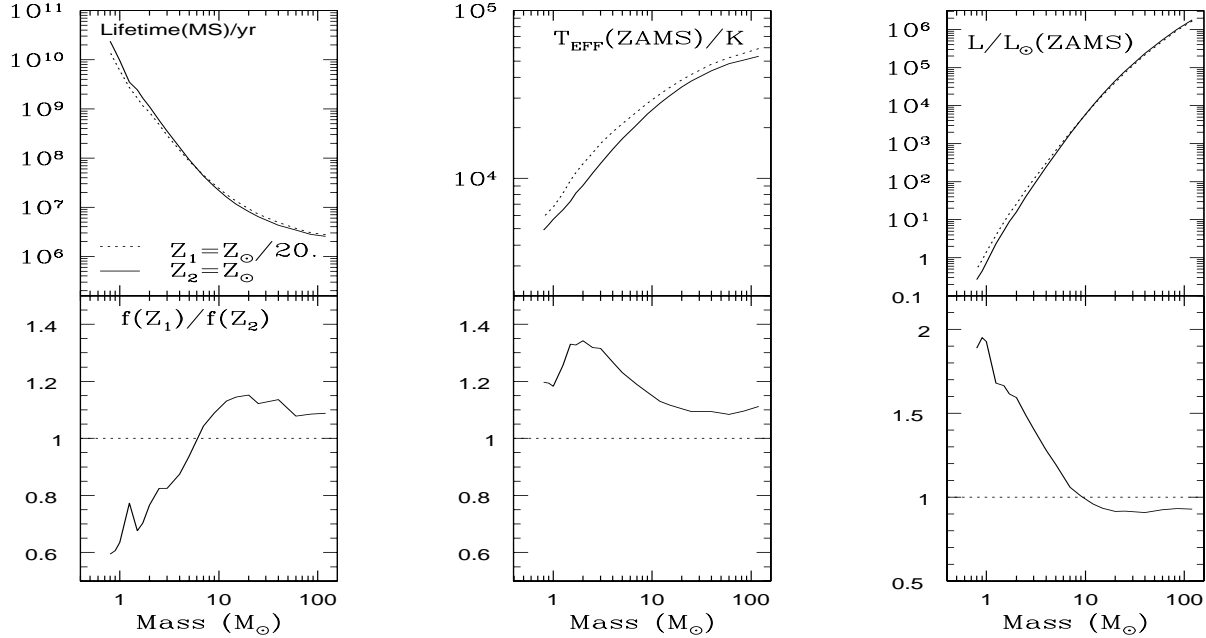


Figure 3. Comparison of Main Sequence (MS) lifetimes (*left*), Zero-Age Main Sequence (ZAMS) effective temperatures (*middle*) and luminosities (*right*) of stars with metallicity $Z_1=Z_\odot/20$ (dotted curves in the *upper* panels) and $Z_2=Z_\odot$ (solid curves in the *upper* panels). In the *lower* panels is displayed the ratio of the corresponding quantities $f(Z_1)/f(Z_2)$. Stars with lower metallicities are in general hotter; those of mass $<5M_\odot$ are more luminous and have shorter lifetimes than their higher metallicity counterparts. All data are from the library of the Geneva stellar evolution tracks (see Sec. 2.2.1).

main-sequence turn-off, He ignition, etc.), allowing for an easy interpolation to other stellar masses and metallicities in the given range.

Stars with $M < 0.8 M_\odot$ and main sequence lifetimes $\tau_{MS} > 13$ Gyr are always attributed their Zero-Age Main Sequence (ZAMS) position, assuming an appropriate mass-luminosity relationship (Baraffe et al. 1997); in view of their very low ZAMS luminosity, their role is negligible in the framework of this work. For $Z < Z_1$ we adopt the tracks for $Z = Z_1$ and for $Z > Z_2$ the tracks for Z_2 . This approximation has a negligible effect on the final results, since very few stars in the disk have metallicities outside that range (see Sec. 3.1 and 3.2).

The metallicity dependence of the stellar tracks and lifetimes may have a considerable impact on the photometric evolution. For that reason, we present in Fig. 3 the main sequence lifetimes, and the zero-age main sequence T_{eff} and L of the adopted models for $Z=Z_\odot$ and $Z=Z_\odot/20$. Stars of low-mass and low metallicity may be $\sim 30\%$ hotter, $\sim 60\%$ more luminous and have $\sim 30\%$ shorter lifetimes than their more “metallic” counterparts.

2.2.2 Stellar spectra

An important contribution to studies of galactic chemical evolution has been recently made by Lejeune et al. (1997). They constructed a homogeneous library of synthetic stellar spectra by compiling different sets of stellar atmosphere models published in the literature. The library covers the wavelength range from 9 nm to 160 μm with a resolution of 1 nm in the UV, 2 nm in the optical and 10 nm in the in-

frared. Stellar spectra are given in the 3-dimensional phase-space of T_{eff} , surface gravity g and metallicity $[\text{Fe}/\text{H}]$, and are uniformly sampled in the range $2500 \text{ K} < T_{eff} < 50000 \text{ K}$, $-1 < \log(g) < 5.5$ and $-3.5 < [\text{Fe}/\text{H}] < +1$. In the temperature range 3 500 K to 50 000 K the models are identical to those of Kurucz (1995). In the range 2 500 K to 3 500 K, composite models of M giants with $[\text{Fe}/\text{H}]$ between -1.5 and +0.5 were constructed, by connecting the Fluks et al. (1994) synthetic spectra with the Bessel et al. (1991) models. Finally, M-dwarf model spectra in the range 2 000 K to 3 500 K were selected from the grid of Allard and Hauschildt (1995). As described in Lejeune et al. (1997), these synthetic spectra have been corrected as to reproduce empirical colour-magnitude relationships, thus eliminating the risk of theoretical errors.

The homogeneity of the library greatly facilitates the calculation of stellar luminosities l_λ , allowing an easy interpolation in stellar mass, metallicity and evolutionary stage. Magnitudes and colours are calculated in the standard photometric system UBVRIJK for each galactic zone.

2.2.3 Extinction by dust

Interstellar dust absorbs light from the stars with a wavelength dependent efficiency and re-emits it in the far infrared (FIR) range. The resulting extinction as a function of wavelength is difficult to evaluate from first principles (see Corradi et al. 1996 for a recent attempt, solving the full radiative transport problem in the case of a disk) and models usually adopt empirical prescriptions.

Extinction, i.e. the quantity $A_\lambda = -2.5 \log(L_\lambda/L_\lambda^0)$ where

L_λ^0 is the intrinsic luminosity of the stellar population calculated in eq. (3) and L_λ the emerging one, depends on both the physical processes involved (absorption and scattering by dust grains) and the geometry of the source. The former is usually parametrized with the introduction of an effective optical depth τ_λ depending on the amount of dust and the absorbing and reflecting properties of grains, while the latter depends on the assumed relative distributions of stars and dust.

The effective optical depth is expressed in terms of the extinction properties observed in the solar neighborhood: i) the extinction in the V band per gas surface density $(A_V/N_H)_\odot = 5.3 \cdot 10^{-22} \text{ mag cm}^2$ (Bohlin et al. 1978) where N_H is the surface density of H (in atoms per cm^2); and ii) the mean extinction curve $(A_\lambda/A_V)_\odot$, adopted here from Natta and Panagia (1984). The dependence on metallicity is introduced by a wavelength independent factor $(Z/Z_\odot)^s$, with $s=1.35$ for $\lambda < 2000 \text{ \AA}$ and $s=1.6$ for $\lambda > 2000 \text{ \AA}$ (adopted from Guiderdoni et al. 1998). The effective optical depth is expressed as:

$$\tau_\lambda = 0.92 a_\lambda \left(\frac{A_\lambda}{A_V} \right)_\odot \left(\frac{A_V}{N_H} \right)_\odot \left(\frac{Z_g}{Z_\odot} \right)^s N_H \quad (5)$$

where a_λ represents a positive contribution to the emerging radiation from light scattered by dust grains, having an albedo ω_λ . We adopt in this work the approximation of Calzetti et al. (1994), concerning a case intermediate between isotropic scattering and purely forward scattering; it turns out that α_λ is given then by:

$$a_\lambda = h_\lambda \sqrt{1 - \omega_\lambda} + (1 - h_\lambda)(1 - \omega_\lambda) \quad (6)$$

where h_λ is a phase factor given by:

$$h_\lambda = 1 - 0.561 \exp \left(- \frac{|\log(\lambda) - 3.3112|^{2.2}}{0.17} \right) \quad (7)$$

with λ expressed in \AA . The grain albedo ω_λ in Calzetti et al. (1994) and in this work is adopted from the work of Natta & Panagia (1984). (For further discussion on the derivation of the above formulae, the reader is referred to Calzetti et al. 1994).

The geometry of the distribution of dust is taken into account as in Xu et al (1997), in a “sandwich model”: one half of the stars is assumed to be mixed with the layer of dust, while the other half lies on each side of this layer, the quarter behind the dust being obscured by the screen. The resulting extinction is then:

$$A_\lambda = -2.5 \log \left(0.25 + 0.5 \frac{1 - e^{-\mu}}{\mu} + 0.25 e^{-\mu} \right) \quad (8)$$

where $\mu = \tau_\lambda / \cos(i)$ and i is the inclination angle ($i=0^\circ$ for face-on galaxies). The first term in parenthesis represents contribution to the emerging luminosity from the stars in front of the dust layer, the second term from the stars mixed with dust and the third one from the stars behind the dust layer.

Extinction should, in principle, be treated with a full radiative transfert code, as e.g. in Corradi et al. (1996). They find that the effect of forward scattering is a very important one, leading to small values of extinction even for large values of the optical depth (e.g. $A_V \sim 0.1 \text{ mag}$ for $\tau_V \sim 4$). We are fully aware that the prescription adopted here is a

very crude one (although it is being routinely adopted in many studies of that kind). For that reason we present below systematically our results for both cases: without (i.e. stellar population only) and with extinction taken into account, according to the adopted prescriptions. In a forthcoming paper we explore the consequences of the radiative transfer treatment of Corradi et al. (1996) on the absorption in various wavelengths.

3 THE EVOLUTION OF THE MILKY WAY

The Milky Way is a heterogeneous system, with at least three components (halo, bulge, disk) having very different chemical, photometric and kinematical properties. A reliable model for the evolution of the Milky Way accounting for those properties does not exist at present. In particular, it is not clear how the various components are related, e.g. whether the evolution of the halo has affected in an important way the one of the bulge or the disk (and vice versa); in fact, it seems that the halo evolution has been completely decoupled from the one of the disk, who evolved quite independently (e.g. Gilmore and Wyse 1998). Neither is it clear whether there has been significant interaction between the various parts of the disk, through large scale gas movements in the radial direction. Despite the development of various models, all these issues are still open.

For the purposes of this work we shall adopt a very simple model for the chemical evolution of the galactic disk, considering its as an ensemble of independently evolving, concentric, rings. In our modelisation we are guided by phenomenology rather than theoretical principles and we try to construct a model that reproduces all the major observational constraints of the Milky Way with a minimum number of free parameters.

3.1 The solar neighborhood

3.1.1 Chemical evolution

In the solar neighborhood (defined as a cylinder of $\sim 1 \text{ kpc}$ radius at a distance $R_S = 8 \text{ kpc}$ from the galactic center), the main observables relevant to chemical evolution are (for a detailed discussion of these observables see PA95 and PS98; see also Table 1 for data and references and Fig. 4 for a graphical presentation of the data):

- i) the current surface densities of gas (Σ_G), stars (Σ_*) and total amount of matter (Σ_T), as well as the current star formation rate Ψ_0 ; a recent analysis of all available data, interpreted in the framework of a consistent mass model for the Milky Way (Mera et al. 1998), shows that there is no compelling evidence for the presence of substantial amounts of sub-stellar objects (brown dwarfs), but a limited amount ($\Sigma_{BD} < 8 \text{ M}_\odot \text{ pc}^{-2}$) cannot be excluded at present.
- ii) the abundances of various elements and isotopes at solar birth ($X_{i,\odot}$) and today ($X_{i,O}$).
- iii) the age-metallicity relationship, traced by the Fe abundance of long-lived, F-type stars.
- iv) the oxygen vs. Fe (O-Fe) relationship, interpreted in terms of a delayed ($\sim 1 \text{ Gyr}$) appearance of SNIa, producing most of galactic Fe.
- v) the metallicity distribution of long-lived G-type stars

Table 1: Main observational data for the solar neighborhood and results of a simple model

Observable	Observed value	Reference	Computed value	Main relevant parameter in the model
<u>Surface densities of:</u>				
Gas	$\Sigma_G = 13 \pm 3 \text{ M}_\odot \text{ pc}^{-2}$	1	12.0	Star Formation History
Stars (visible)	$\Sigma_* = 35 \pm 5 \text{ M}_\odot \text{ pc}^{-2}$	2	34.5	
Stars (visible+remnants)	$\Sigma_* = 43 \pm 5 \text{ M}_\odot \text{ pc}^{-2}$	3	39.9	[Stellar IMF
Total (stars+gas)	$\Sigma_T = 51 \pm 6 \text{ M}_\odot \text{ pc}^{-2}$	4	53.0	
Gas fraction	$\sigma_G = 0.15\text{--}0.25$		0.22	+ Infall Rate
Star formation rate	$\Psi_o = 2\text{--}5 \text{ M}_\odot \text{ pc}^{-2} \text{ Gyr}^{-1}$	5	3.2	+
Past average SFR	$\langle \Psi \rangle \sim 3 \text{ M}_\odot \text{ pc}^{-2} \text{ Gyr}^{-1}$		2.6	Star Formation Law]
SNII rate	$0.02 \text{ pc}^{-2} \text{ Gyr}^{-1}$	6	0.018	
Present Day Mass Function (PDMF)	Low mass part: uncertain (flatter than $X=1.35$)	7,8		IMF + SFR
<u>Abundances</u>				Stellar yields
At $T_0\text{--}4.5 \text{ Gyr}$	$X_{i,\odot}$ $X_{O,\odot} = 9.20 \cdot 10^{-3}$ $X_{Fe,\odot} = 1.17 \cdot 10^{-3}$	9,10	$7.6 \cdot 10^{-3}$ $1.1 \cdot 10^{-3}$	
At $T_0 \sim 13.5 \text{ Gyr}$	$X_{i,0} \sim X_{i,\odot}$	11, 12		
O/Fe vs Fe/H :	Decline for $[\text{Fe}/\text{H}] > -1$	13		SN Ia rate
Age-metallicity (Z vs. t)	Slow increase of Z Dispersion (?)	13		Star formation + yields
Metallicity distribution of G-dwarf stars	Narrow Peaked at $[\text{Fe}/\text{H}] \sim -0.1$	14,15		Infall rate
<u>Luminosities:</u>				
	$L_B = 20.0 \pm 2.0 \text{ L}_{B\odot} \text{ pc}^{-2}$	16	26.8	Star Formation History
	$L_V = 22.5 \pm 3.0 \text{ L}_{V\odot} \text{ pc}^{-2}$	17	25.9	+
	$L_K = 68.0 \pm 23. \text{ L}_{K\odot} \text{ pc}^{-2}$	18	85.36	Stellar tracks
<u>Colours:</u>				
	B-V = 0.85 ± 0.15 (0.63 ± 0.1)	16 19	0.71	Stellar Spectra Extinction

References: 1. Kulkarni and Heiles 1987 ; 2. Gilmore et al. 1989 ; 3. Mera et al. 1998 ; 4. Sackett 1997 ; 5. Rana 1991 ; 6. Tammann et al. 1994 ; 7. Scalo 1986 ; 8. Kroupa et al. 1993 ; 9. Anders and Grevesse 1989 ; 10. Grevesse et al. 1996 ; 11. Cunha and Lambert 1994 ; 12. Cardelli and Federmann 1997 ; 13. Edvardsson et al 1993 ; 14. Rocha-Pinto and Maciel 1996 ; 15. Wyse and Gilmore 1995 ; 16. van der Kruit 1986 ; 17. Pagel 1997 ; 18. Kent et al. 1991 ; 19. Robin 1998

(Fig. 4c), showing that very few of them were formed at $[\text{Fe}/\text{H}] < -0.7$ (1/5 solar) or $[\text{O}/\text{H}] < -0.5$ (1/3 solar).

vi) the present day mass function (PDMF), resulting from the stellar IMF and the SFR history; this observable is rarely considered in studies of the local chemical evolution (with the exception of Ferrini et al. 1994). However, the resulting theoretical PDMF constitutes an important consistency check for the adopted SFR and IMF.

The simple model described in Sec. 2.1 can reproduce the above constraints, as can be seen in Figs. 4 and 5a. The adopted SFR and infall rates lead to a current gas surface density of $\Sigma_G \sim 10 \text{ M}_\odot \text{ pc}^{-2}$ and to a final stellar surface density of $\Sigma_* \sim 35 \text{ M}_\odot \text{ pc}^{-2}$, both compatible with the observations. The final amount of stellar remnants ($\Sigma_R \sim 7 \text{ M}_\odot \text{ pc}^{-2}$, for the sum of white dwarfs + neutrons stars + black holes) is slightly smaller than the current gas amount. Models of the local chemical evolution cannot avoid producing this amount of stellar remnants, i.e. about 15% of the local

surface density (a different IMF would slightly change this figure).

With the adopted infall and star formation rates, a current SFR $\sim 3 \text{ M}_\odot \text{ pc}^{-2} \text{ Gyr}^{-1}$ is obtained at $T=13.5 \text{ Gyr}$, again in agreement with observations. Those ingredients, combined with the adopted IMF and stellar yields lead to a local metallicity close to the solar one 4.5 Gyr ago and slightly higher today (Fig. 4b). It should be noted here that observations of CNO abundances in young stars and gas in Orion show that the metallicity of this young region is lower than solar (Cunha and Lambert 1994, Cardelli and Federmann 1997), a result which is difficult to interpret in conventional chemical evolution models (see e.g. PA95); imperfect or non-instantaneous mixing could, perhaps, help explain this observable, as well as the scatter in the age-metallicity relationship (e.g. Coppi 1997, Thomas et al. 1998).

The current SN II rate in the solar neighborhood is found to be compatible with the estimate of Tammann et al. 1994 (fig. 8f): $2 \cdot 10^{-11} \text{ pc}^{-2} \text{ yr}^{-1}$. The SN Ia rate is adjusted

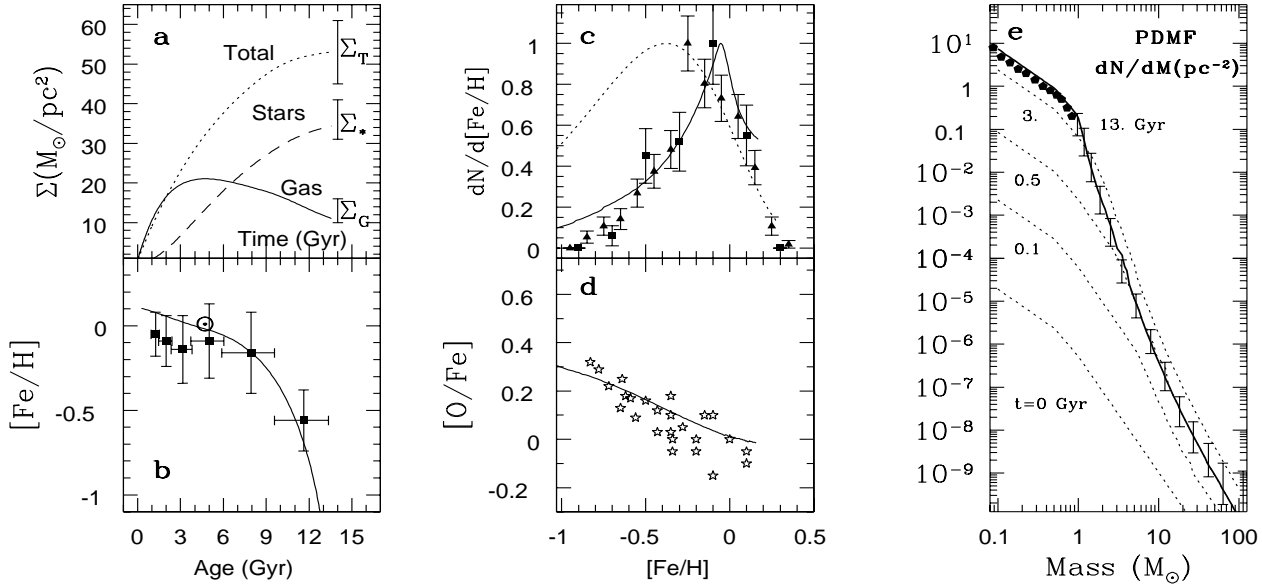


Figure 4. Results of the chemical evolution model for the solar neighborhood and comparison to observations (see Sec. 3.1.1 and Table 1 for References). **a:** Surface densities of stars, gas and total amount of matter as a function of time (present day data within vertical error bars); **b:** Age-Metallicity relationship; **c:** G-dwarf differential metallicity distribution, with results from our model (solid curve) and a closed-box model (dotted curve) shown for comparison; **d:** Oxygen vs. Fe relationship; **e:** Evolution of the Present Day Mass Function (dotted curves, at various instants) to the observed PDMF of the final one (solid curve) to the observed PDMF of Scalo (1986, vertical error bars for $M > 1 M_{\odot}$ stars) and of KTG93 (filled symbols, for low mass stars); for $M > 1 M_{\odot}$ the KTG93 IMF coincides with the one of Scalo (1986). Obviously, at time $t=0$ the PDMF coincides with the adopted IMF; at $t=13$ Gyr this is true for low-mass stars.

to reproduce the observed decline of O/Fe in the local disk (Fig. 4d). The introduction of this delayed Fe source leads to an age-metallicity relationship somewhat steeper than (but still compatible with) the observations (Fig. 4b).

The differential metallicity distribution (DMD) of G-dwarfs constitutes one of the strongest constraints for the evolution of the solar neighborhood. It represents the number of long-lived stars per unit logarithmic metallicity interval and can be evaluated as:

$$\frac{dN_G}{d[\text{Fe}/\text{H}]} = \frac{\alpha_G \Psi(t) dt}{d[\text{Fe}/\text{H}]} \quad (8)$$

where $\Psi(t)$ is the SFR at time t and $dN_G = \alpha_G \Psi(t) dt$ is the number of G-type stars born with metallicities between $[\text{Fe}/\text{H}]$ and $[\text{Fe}/\text{H}] + d[\text{Fe}/\text{H}]$; α_G is the fraction of G-type stars in the IMF. Expression (8) relates explicitly the SFR history and the age-metallicity relationship to the DMD of G-dwarfs. If the latter two relationships were accurately known, the local SFR could be easily derived (Prantzos 1998a), but current observational uncertainties prevent from such a derivation. As can be seen from Fig. 4c the local G-dwarf DMD is nicely reproduced with the slow in-fall adopted in our model. Notice that the use of metallicity dependent stellar lifetimes cannot solve the G-dwarf problem (e.g. Bazan and Mathews 1990; Rocha-Pinto and Maciel 1997).

Finally, in Fig. 4e we present also the evolution of the Present Day Mass Function (PDMF), at times 0., 0.1, 0.5, 3 and 13 Gyr from the beginning and we compare the final result with the observed PDMF of Scalo (1986, in the mass range $1-100 M_{\odot}$) and KTG93 (low mass stars only). In the

mass range $< 1 M_{\odot}$ (where the shape of the PDMF coincides with the one of the IMF), the adopted IMF of KTG93 differs from the flatter ones of Scalo (1986), Gould et al. (1997) and Reid and Gizis (1997), but it is compatible with the one favoured by Haywood et al (1994); the Salpeter IMF is steeper than any of those IMFs. In the high mass range, the shape of the PDMF is mainly determined by the stellar lifetimes (for small variations of the IMF slope X) and it is not surprising that the results of Scalo (1986) are recovered.

Despite the satisfactory agreement of our model with the observations, we wish to emphasize that the solution is by no means unique (see Tosi 1988), i.e. some other combinations of the input parameters may also lead to acceptable results (see Tosi 1998 for a comparison of different models). Notice, however, that the constraints are relatively tight and do not allow for a wild variation in the input parameters. In particular, the metallicity distribution strongly suggests a slow formation of the local disk; this is corroborated by the observed current local SFR (Prantzos 1998a), which is not very different from the past average one ($\text{PASFR} = \Sigma_*/T \sim 3 M_{\odot} \text{pc}^{-2} \text{Gyr}^{-1}$). A very high early SFR, declining to very low current values, is not compatible with those data.

3.1.2 Photometric evolution

The set of available observational constraints concerning the photometric evolution of the solar neighborhood is much smaller than the corresponding one for its chemical evolution (second part of Table 1 and references therein). The local surface brightness is estimated to $L_V = 22.5 \pm 3 L_{V\odot} \text{pc}^{-2}$. Combined to the observed star surface density of $\Sigma_* =$

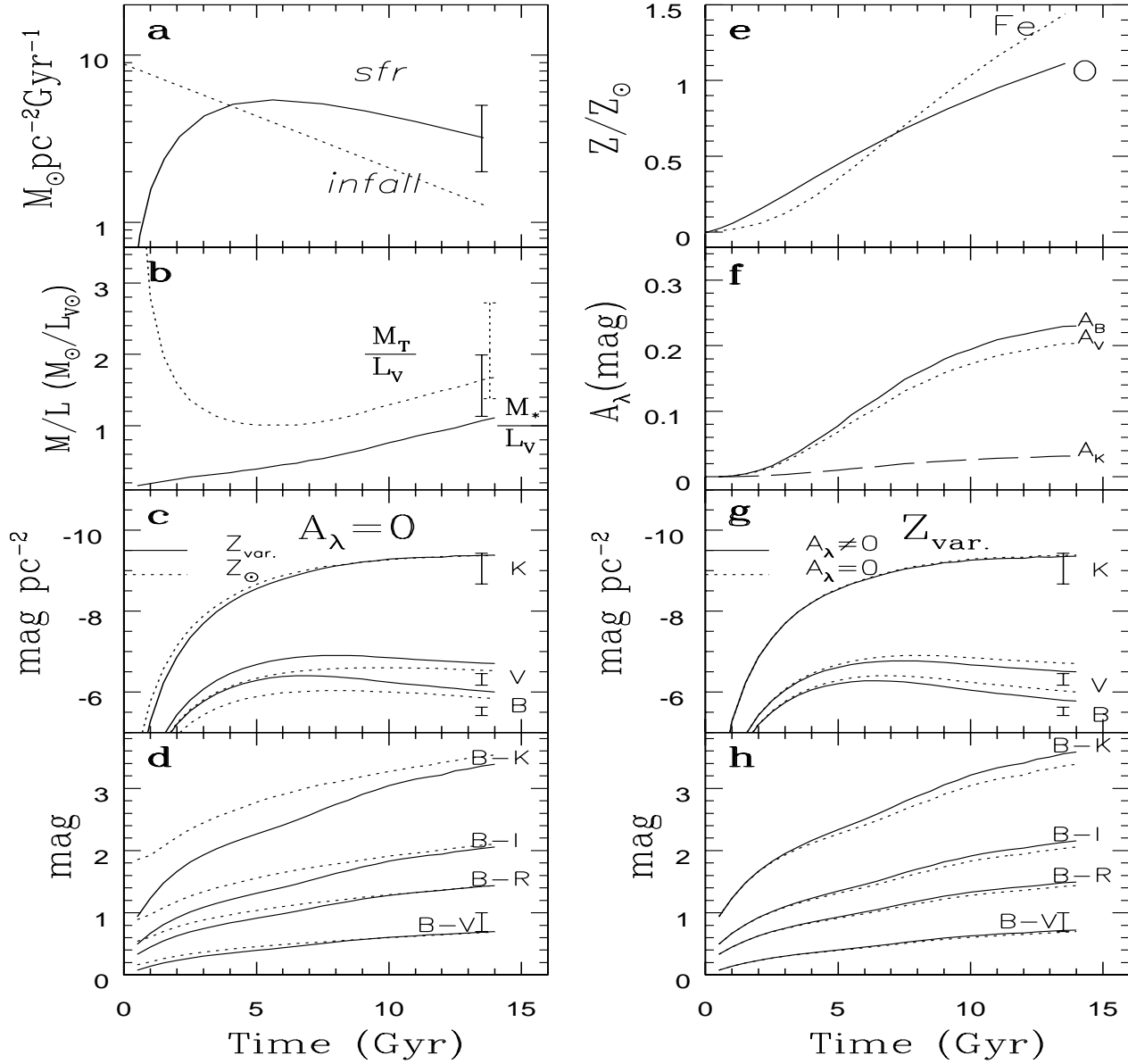


Figure 5. Results of the chemo-photometric evolution model for the solar neighborhood (Sec. 3.1.2) and comparison of the values at $T=13.5$ Gyr to observations (with vertical *error bars*). The effects of metallicity dependence of the stellar tracks are presented in panels **c** and **d**, whereas those of extinction in panels **g** and **h**. **a**: Star formation and infall rates; **b**: M/L_V ratio for the total mass (*dotted* curve) and the stellar mass (*solid* curve); **c**: Surface brightness in the K, V and B bands, obtained with the SFR of Fig. 5a, no extinction and stellar tracks of constant metallicity Z_\odot (*dotted* curve) or variable metallicity (*solid* curve); **d**: Corresponding evolution of colours (*solid* curve: variable metallicity stellar tracks, *dotted* curve: tracks with $Z = Z_\odot$); **e**: Abundances of Fe (*dotted* curve) and O (*solid* curve) on a linear scale, the latter been adopted as tracer of metallicity for the calculation of extinction according to Eq. 8; **f**: Extinction in the B, V and K bands; **g**: Surface brightness in the K, V and B bands, obtained with the SFR of Fig. 5a, stellar tracks of variable metallicity and extinction neglected (*dotted* curve) or included (*solid* curve); **h**: Corresponding evolution of colours (extinction neglected: *dotted* curves; extinction included: *solid* curves). The *solid* curves in figures 5g and 5h represent our final complete model for the local photometric evolution.

$35 \pm 5 \text{ M}_\odot \text{pc}^{-2}$, it leads to a local stellar mass/light ratio of $M/L_V = 1.2\text{--}2$. (in solar units); if the total local surface density $\Sigma_T \sim 51 \pm 5 \text{ M}_\odot \text{pc}^{-2}$ is adopted instead, M/L_V is found to be $\sim 1.8\text{--}2.8$. Notice also the uncertainty in the local

$B - V$ value, equal to 0.84 ± 0.15 (van der Kruit 1986) or to 0.63 (Robin 1998).

The results of our model for the photometric evolution of the solar neighborhood appear in Fig. 5. In Fig. 5b appears the evolution of the M/L_V ratio where L_V is the lumi-

osity of the stellar population calculated with metallicity-dependent stellar tracks and with no extinction taken into account. The two curves correspond to M representing either the stellar mass only or the total mass (i.e. stars + gas + stellar remnants); in both cases, the obtained value at $T=13.5$ Gyr is on the low side of the observed range.

The effects of the metallicity dependence of the adopted stellar tracks are illustrated in Fig. 5c (luminosity evolution) and 5d (colour evolution); the results correspond again to the luminosity of the stellar population alone, i.e. without any extinction. It can be seen that the adoption of metallicity-dependent tracks leads to systematically larger B - and V - luminosities than the case with $Z=\text{const}=Z_{\odot}$ tracks, especially towards the middle of the galactic evolution where the differences can attain 0.5 mag. Towards the end of the evolution the differences are small, since the metallicity has increased to $\sim Z_{\odot}$ and the tracks with Z_{\odot} are quite appropriate. Notice that the final B - and V - luminosities are barely compatible with the observed local ones, but if extinction is taken into account (see next paragraph) the agreement becomes satisfactory. Notice also that the K - band luminosity is very slightly affected by these considerations. As a result, the colour evolution of e.g. $B-K$ depends very strongly on the adopted stellar tracks. As can be seen in Fig. 5d, the early $B-K$ is “redder” by almost 1 mag when metallicity-independent tracks are considered. This illustrates dramatically the importance of adopting metallicity-dependent stellar tracks and calculating in a self-consistent way the photometric and chemical evolution of a galaxy. On the other hand, the $B-V$ colour is very slightly affected by the metallicity dependence of the tracks; the final value (0.69 with no extinction, Fig. 5d) is quite close to the observed (but very uncertain!) value in the solar neighborhood.

On the right part of Fig. 5 are illustrated the effects of extinction on the results of our calculation. According to the adopted prescription, the optical depth depends in a sensitive way on metallicity (Eq. 5); one should worry then about the appropriate metallicity tracer, since O and Fe evolve in rather different ways (Fig. 5e). Since the adopted stellar tracks of Geneva are parametrised by the total metallicity, dominated by oxygen, we adopt this element here as metallicity tracer in the extinction law. Another reason is that our study concerns also other galactic regions (and, in a forthcoming paper, other spirals as well) for which there are no data concerning their Fe evolution neither the SNIa rate (contrary to what happens in the solar neighborhood); since the evolution of the oxygen abundance is tidely related to the star formation rate, we feel that this element is a safer tracer of metallicity (at least from the theoretician’s point of view).

The evolution of the extinction in various wavelengths (Eq. 8) appears in Fig. 5f: it is negligible in all wavelengths in the beginning (because of low metallicity and gas amount); it is always negligible in the K - band, but can reach 0.3 mag in the B - and V - bands. Although the metallicity increases steadily, extinction levels out at late times, because it depends also on the surface gas density, which decreases lately (Fig 5a). Fig. 5g displays the effect of extinction on luminosity: a better agreement with the current local V - and (in particular) B - luminosity is obtained when extinction is taken into account. Finally, Fig. 5h displays the correspond-

ing evolution of various colours; $B-V$ is not affected by extinction (since both the B - and V - bands are affected in a similar way), while $B-K$ increases by ~ 0.25 mag.

From Figs. 5a,g,h it becomes clear that the effect of extinction on the local photometric evolution is small, mainly because of the relatively small current amount of gas. The other parameters of the model (shape of the IMF, SFR history) have a stronger impact on that evolution. Notice, however, that this is not the case for inner galactic regions having larger gaseous and metal amounts (see next Section).

As a final comment, we note that the effect of metallicity dependent stellar tracks is most important in the early galactic evolution, whereas the effects of extinction become (relatively) important only at late times.

3.2 The Milky Way disk

3.2.1 Chemical evolution

Contrary to the case of the solar neighborhood, the available observations for the Milky Way disk offer information mainly about its current status, not its past history. The main observables relevant to chemical evolution are (see PA95 and PS98 for a more detailed discussion; also Table 2 for data and references):

i) The total mass of gas and stars in the disk ($M_G \sim 6-8 \cdot 10^9 M_{\odot}$ and $M_{\star} \sim 4-5 \cdot 10^{10} M_{\odot}$, respectively); the total current SFR ($\sim 3-6 M_{\odot} \text{ yr}^{-1}$) and the current supernova rates ($\sim 1-2$ SNII/century and $\sim 0.2-0.4$ SNIa/century, respectively, as suggested by observations of external spirals; the uncertainty on the value of the Hubble constant and on the exact spectral type of the Milky Way - Sb or Sbc - prevents from giving a precise value). Notice that those quantities are often mentioned as constraints to (and predictions of) one-zone models of the Galaxy, assumed to reflect the evolution of the whole disk. This is obviously wrong, since the disk is a heterogeneous system, as the observed gradients suggest (see points iii-vi below). A multi-zone model with different SFR histories in its various zones should be obviously used. In fact, observations of external spirals give rather the SN frequency in SNU (i.e. in number of SN per century and per $10^{10} L_{B\odot}$ in Table 2); knowledge of the current L_B for the Milky Way allows then to infer its current SN frequency. However, a succesful model of the Milky Way should reproduce in a self-consistent way *both* its SN frequency and L_B luminosity.

ii) The current gas profile, dominated by the molecular ring at galactocentric distance $R \sim 4-5$ kpc and by HI of roughly constant surface density at distances 6-14 kpc (Dame 1993 and Fig. 2).

iii) The stellar profile, exponentially decreasing outwards. The value of the characteristic scalelength is still under debate, but recent studies converge towards low scalelengths, around 2.5-3 kpc (Sackett 1997). A recent analysis of the COBE data (Freudenreich 1998) also points to a scalelength $h=2.6$ kpc. The combination of observables (ii) and (iii) leads to a gas fraction profile steeply decreasing in the inner disk, suggesting that the star formation efficiency has been larger in those regions than in the outer disk.

iv) The current SFR profile (traced by the surface density of pulsars and supernova remnants or the H_{α} emissivity profile), strongly decreasing outwards (Fig. 2 and references

Table 2: Main observational data for the Milky Way disk and results of a simple model

Observable	Observed value	References	Computed value	Main relevant parameter
<u>Total mass of:</u>				
Gas	$M_G : 6\text{--}8 \cdot 10^9 M_\odot$	1,2,3	$8 \cdot 10^9$	Same ingredients
Stars	$M_* : 4\text{--}5 \cdot 10^{10} M_\odot$	1,4	$3.8 \cdot 10^{10}$	
Gas fraction	$\sigma_G \sim 0.15$		0.15	as for
<u>Star formation</u>				
Current SFR	$\Psi_o : 2\text{--}6 M_\odot \text{ yr}^{-1}$	1,7	1.9	Solar
Frequency of SNII	0.55–1.0 SNU	8,9	0.61	
Frequency of SNIa	0.12–0.23 SNU	8,9	0.16	
Infall rate	$f < 2 M_\odot \text{ yr}^{-1}$	7	0.64	Neighborhood
				plus
<u>Profiles</u>				
Gas	$\Sigma_G(R)$	1, 2		Radially dependent
Stars	$\Sigma_*(R) \propto \exp^{-R/H}$ ($H \sim 2.5 \text{ kpc}$)	4,5,6,16		
SFR	$\Psi(R)$	1, 14		SFR $\Psi(R)$
Abundances in gas and B-stars	$X_i(R)$ $d[\text{O}/\text{H}]/dR \sim -0.08 \text{ dex/kpc}$	10,11	-0.07	Infall $f(R)$
<u>Luminosities:</u>				
	$L_B = 1.8 \pm 0.3 \cdot 10^{10} L_{B\odot}$	12	$1.8 \cdot 10^{10}$	Same ingredients
	$L_V = 2.1 \pm 1.0 \cdot 10^{10} L_{V\odot}$	5	$2.0 \cdot 10^{10}$	
	$L_K = 6.7 \cdot 10^{10} L_{K\odot}$	13	$7.5 \cdot 10^{10}$	as for Solar
<u>Colours:</u>	B-V ~ 0.8	12	0.78	Neighborhood
<u>Scalelengths:</u>				
	$H_B = 4\text{--}5 \text{ kpc}$	13	3.9	Photometry
	$H_K = 2.3\text{--}2.8 \text{ kpc}$	14,15	2.6	

References: 1. Prantzos and Aubert 1995; 2. Dame 1993; 3. Kulkarni and Heiles 1987; 4. Mera et al. 1998; 5. Sackett 1997; 6. Robin et al. 1992 ; 7. Pagel 1997; 8. Tammann et al. 1994; 9. Capellaro et al. 1997; 10. Shaver et al. 1983; 11. Smart and Rolleston 1997; 12. van der Kruit 1986; 13. Kent et al. 1991; 14. Wang and Silk 1994; 15. Freudenreich 1998 ; 16. Ruphy et al. 1996

therein). Notice that the SFR profile does not follow the molecular or the total (molecular+atomic) one, i.e. the SFR is not simply proportional to some power of the gaseous profile.

v) The current metallicity profile, usually traced by oxygen observed in HII regions (Shaver et al. 1983, Vilchez and Esteban 1996), young planetary nebulae (Allen et al. 1998), and B-stars (Smart and Rolleston 1997, Gummersbach et al. 1998), showing a gradient of $d[\text{O}/\text{H}] \sim -0.08 \text{ dex/kpc}$.

Notice that, since there are essentially no constraints on the past history of the Milky Way disk (i.e. no age-metallicity relations or metallicity distributions are available for other regions) there is much more freedom in its modelisation than in the case of the solar neighborhood. Still, it is meaningful to construct models, insofar as the number of parameters used is considerably smaller than the constraints (i-v) above.

In our previous works (PA95, PS98) we presented a simple model of that kind, i.e. one with the same physics as for the solar neighborhood and with a radial dependence in the star formation rate $\text{SFR}(R)$ and the infall timescale $\tau(R)$. As discussed in Sec. 2.1.1, the adopted radial dependence has a physical basis (i.e. large scale instabilities in rotating disks for the SFR and inside-out formation of the disk for

the infall timescale τ). It turns out that with this simple parametrisation the model reproduces reasonably well the constraints (i-v), as can be seen in Fig. 6. Among those, the gaseous profile is the most difficult to reproduce by models of that kind; we obtain a rather broad peak around 5 kpc, in rough agreement with observations. It is difficult to ask more from such a simple model, especially since other factors may have shaped the gaseous profile in the inner Galaxy (like e.g. the presence of a bar inducing radial inflows and enhancing the SFR there). Notice that this difficulty of the simple models has already been pointed out in Wang (1990).

The model also reproduces reasonably well the total current SFR and supernova rates (Table 2), as well as various other quantities. This is a rather encouraging success, since the number of the new constraints is much larger than the number of the new parameters. In fact, the stellar profile is essentially determined by the boundary conditions (the adopted $\Sigma_T(R)$ profile in the normalisation of Equ. 3), but the form of the star formation rate $\Psi(R)$ and infall timescale $\tau(R)$ (two parameters) account then for the observed gaseous, SFR and oxygen profiles, as well as the other results in Table 2 and Fig. 6.

The model can then be used with some confidence for making further predictions. Some of them have been anal-

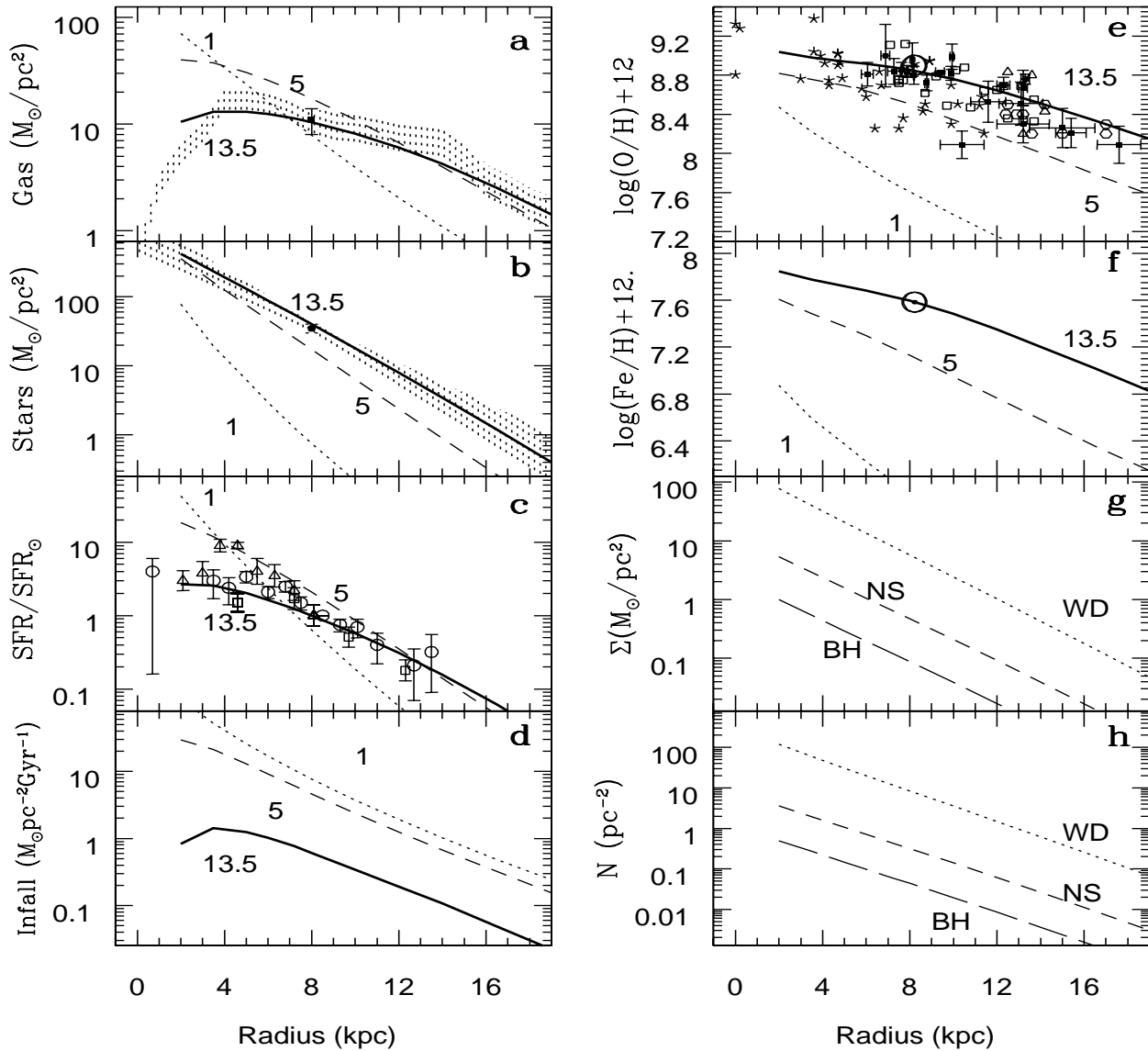


Figure 6. Results of the chemical evolution model for the Milky Way disk (Sec. 3.2.1) and comparison to observations (see Table 2 for references). **a:** Gas profile at 1 Gyr (dotted curve), 5 Gyr (dashed curve) and 13.5 Gyr (thick solid curve) and comparison of the latter to observations of the current gaseous profile (grey area, normalised to the local gas surface density, within error bars); **b:** Stellar profile at 1 Gyr (dotted curve), 5 Gyr (dashed curve) and 13.5 Gyr (thick solid curve) and comparison of the latter to observations of the current stellar profile (grey area, within two exponential disks of scalelengths 2.2 and 2.6 kpc, respectively and normalised to the current local star surface density, within error bars); **c:** Star formation rate, normalised to its current value at $R_S=8$ kpc at 1 Gyr (dotted curve), 5 Gyr (dashed curve) and 13.5 Gyr (thick solid curve) and comparison of the latter to observations (see Fig. 2 and references therein for observational data); **d:** Profile of the infall rate at 1 Gyr (dotted curve), 5 Gyr (dashed curve) and 13.5 Gyr (thick solid curve); **e:** Oxygen abundance profile at 1 Gyr (dotted curve), 5 Gyr (dashed curve) and 13.5 Gyr (thick solid curve) and comparison of the latter to observations; **f:** Iron abundance profile at 1 Gyr (dotted curve), 5 Gyr (dashed curve) and 13.5 Gyr (thick solid curve); **g:** Current surface densities (by mass) of: white dwarfs (WD, dotted curve), neutron stars (NS, short-dashed curve) and black holes (BH, long-dashed curve); **h:** Current surface densities (by number) of: white dwarfs (WD, dotted curve), neutron stars (NS, short-dashed curve) and black holes (BH, long-dashed curve).

used elsewhere (see e.g. Prantzos 1996 for the importance of the deuterium abundance profile for our understanding of the past history of the disk, or Prantzos et al. 1996 on the evolution of the CO isotopic profiles). In Fig. 6 we present two more predictions of the model concerning a) the evolution of the metallicity gradients in the disk and b) the surface

density of compact objects (white dwarfs, neutron stars and black holes) as a function of galactocentric distance.

The evolution of the metallicity gradient is an important issue in studies of the evolution of galactic disks (see e.g. Köppen 1994 and references therein). In particular, the flattening of the metallicity profile is supporting the idea

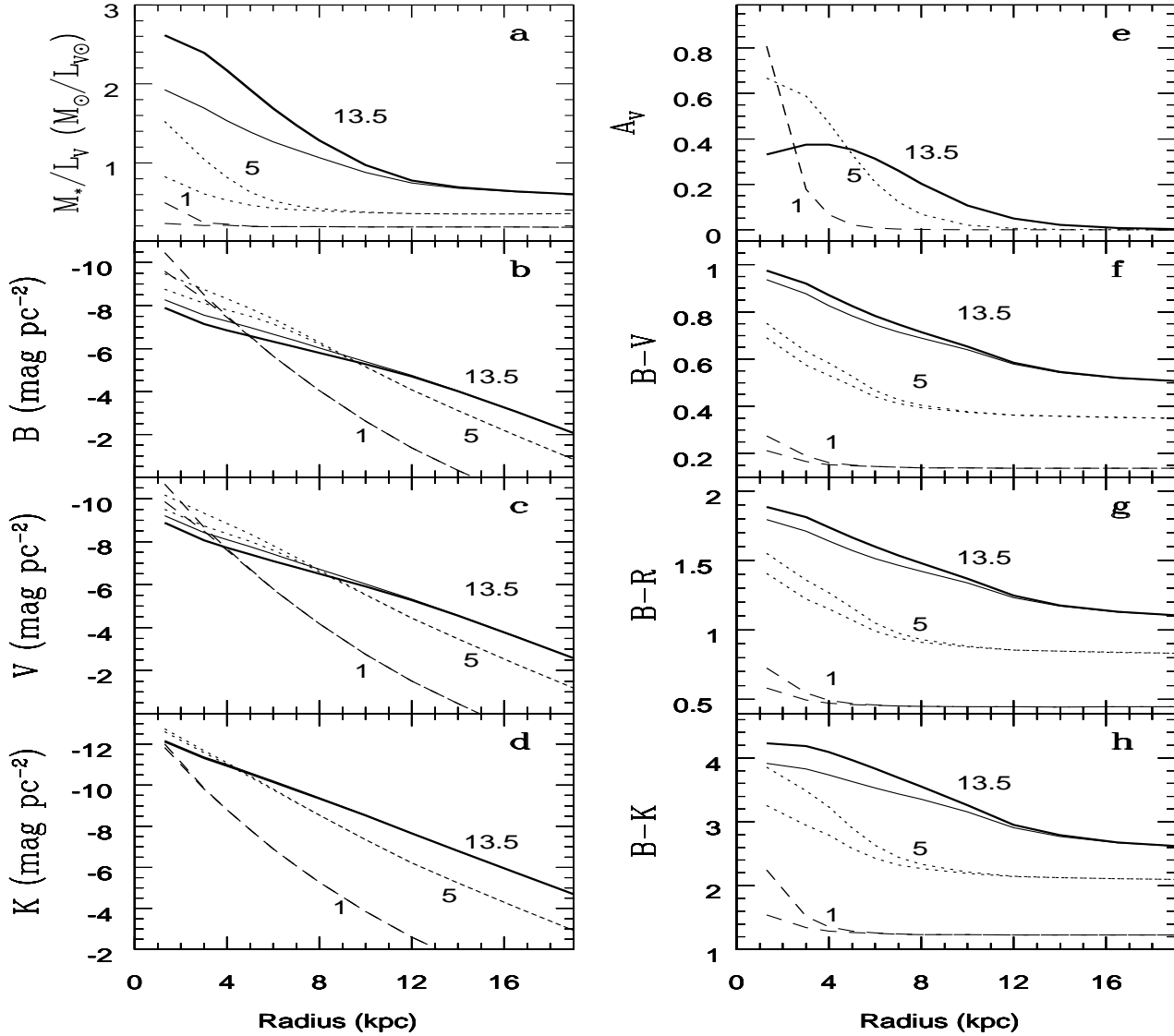


Figure 7. Results of the chemo-photometric evolution model for the Milky Way disk (Sec. 3.2.2) with metallicity-dependent stellar tracks. In each panel, three curves are given, corresponding to profiles at times $t=1$ Gyr (*dashed* curve), 5 Gyr (*dotted* curve) and 13 Gyr (*thick solid* curve), respectively; bifurcation of the curves (mostly in the inner disk) correspond to extinction neglected (upper part of the bifurcation in the surface brightness profiles, lower part in the colour profiles and M/L_V ratio) or included (lower part in the surface brightness profiles, upper part in the colour profiles and M/L_V ratio). **a:** Stellar M/L_V ratio ; **b:** B – surface brightness (the final exponential disk has a scalelength of $H_B \sim 3.9$ kpc but breaks down outside ~ 13 kpc ; **c:** V – surface brightness ; **d:** K – surface brightness (the final exponential disk has a scalelength of $H_K \sim 2.6$ kpc, i.e. shorter than the B –disk, in fair agreement with observations ; **e:** Extinction in the V – band ; **f:** Evolution of $B - V$ colour profile ; **g:** Evolution of $B - R$ colour profile ; **h:** Evolution of $B - K$ colour profile. In all the figures, the thick dotted curve presents our final complete model. i.e. with extinction taken into account. It is clear that extinction enhances but does not create colour gradients, especially at late times.

of inside-out formation of the disk (since the inner regions arrive to the endpoint of their evolution more rapidly than the outer ones). In the case of our model, this evolution is clearly seen in Fig. 6a,b,c, where the gaseous, stellar and SFR profiles are given at three times (1, 5 and 13.5 Gyr respectively). Unfortunately, the existing abundance data on stars and planetary nebulae of various ages do not allow at present to conclude on the behaviour of the metallicity profile on observational basis (see Molla et al. 1997 for a

thorough discussion of the data and the associated uncertainties). The recent works of Molla et al. (1997) and Allen et al. (1998) conclude that the O-abundance profile should become flatter with time and that it should evolve very little in the past ~ 6 Gyr, on the basis of models not very different from ours. We confirm these conclusions, as can be seen in Fig. 6e. Also, in agreement with Molla et al. (1997) we find that the Fe-abundance profile is steeper than the one of oxygen at any age (Fig. 6f); this is due to the enhanced ratio of

SN Ia to SN II in the inner disk, resulting from the adopted prescription for the SN Ia rate (see Sec. 2.1.4). As already stressed in PA95, the evolution of the O vs. Fe abundance profiles is crucial to our understanding of the past SN Ia history in other regions of the galactic disk.

The last two pannels of Fig. 6 display the final profiles of the surface densities of stellar remnants, by mass (Fig. 6g) and by number (Fig. 6h), respectively. As already discussed in Sec. 3.1.1, the local surface density of stellar remnants is found to be slightly lower than the corresponding gaseous one. Comparison to Fig. 6a shows that in the inner disk stellar remnants dominate the gas (i.e. inside ~ 5 kpc). In Fig. 6h it is seen that in the inner Galaxy number densities of stellar remnants (always dominated by white dwarfs) can reach $\sim 100 \text{ pc}^{-2}$. These numbers, resulting from our model, may have important implications for a) the resulting M/L_V profile (see Sec. 3.3.2); b) statistics of experiments concerning micro-lensing events in the direction of the galactic bulge (e.g. Han and Chang 1998 and references therein); or c) the detection of neutron stars and black holes in binary systems (e.g. Romani 1998, Bethe and Brown 1998). The resulting total current numbers in our model are: $\sim 10^{10}$ white dwarfs, $5 \cdot 10^8$ neutron stars and $\sim 5 \cdot 10^7$ black holes in the Galaxy. The numbers for neutron stars and black holes are lower by a factor of ~ 2 than the corresponding ones of Timmes et al. (1996), one of the reasons being the use of the Salpeter IMF in that work vs. the more realistic KTG93 IMF in our model.

3.2.2 Photometric evolution

As in the case of the solar neighborhood, the set of photometric data for the Milky Way disk is smaller (and more uncertain) than the corresponding one for chemical evolution (Table 2). In particular, there is considerable uncertainty about the scale-length in the various wavelengths; it is clear, however, that scalelengths are larger in the shorter wavelengths (e.g. $\sim 4\text{--}5$ kpc in the $B\text{--}$ band vs. $\sim 2.3\text{--}3$ kpc in the $K\text{--}$ band). One of the main results of this section concerns precisely this issue.

The evolution of the luminosity profile in several wavelengths and of the associated colour profiles appears in Fig. 7, for three different epochs: 1 Gyr, 5 Gyr and 13.5 Gyr, so that a direct comparison is possible with the corresponding profiles of gas, stars, SFR and metallicity (Fig. 6). Our calculations are performed with metallicity dependent stellar tracks and results are displayed with and without extinction.

The luminosity profiles clearly reflect the inside-out formation of the disk, one of the basic ingredients of our model: in all wavelengths the disk is smaller and more compact in early times. The $K\text{--}$ band profile reflects better the stellar profile of Fig. 6b than the shorter wavelengths; its scale-length increases to a final value of ~ 2.6 kpc, in fair agreement with the observationally deduced one (Table 2). On the other hand, the $B\text{--}$ profile is generally flatter, in particular in the inner disk and follows closely (albeit not perfectly) the SFR profile (Fig. 6c); both profiles reflect the young stellar population and flatten in the inner disk at late times because of the exhaustion of gas supply in that region. The final profile of L_B is exponential, with a scalelength ~ 4 kpc between 3 and 13 kpc, i.e. for about 3 scalelengths. Outside

13 kpc the final $B\text{--}$ profile steepens, as does the corresponding SFR profile (Fig. 6c).

The stellar M/L_V profile (Fig. 7a) has a uniform value ~ 0.2 (in solar units) at $t=1$ Gyr; its value rises more rapidly in the inner disk (where it reaches a value of ~ 2 at 13.5 Gyr), than in the outer disk. As with extinction and colour profiles (see next paragraphs) the final M/L_V profile is very flat outside ~ 13 kpc. The reason is that in the inner disk, a large number of the stars emitting in the $V\text{--}$ band are created early on and are dead by $t=13.5$ Gyr, contributing to M but not to L_V . In the outer disk, most of those stars are created relatively late (because of the inside-out star formation) and are still shining.

Extinction (Fig. 7e) plays some role in the inner disk, where A_V can reach ~ 0.4 mag (compared to ~ 0.2 mag in the solar neighborhood; see Fig. 5f). Contrary to the solar neighborhood, where A_V remains \sim constant in the past ~ 5 Gyr (since the effect of gas depletion is compensated by a small increase in metallicity), in the inner disk A_V decreases with time, since the important gas depletion is not compensated by a corresponding metallicity increase (metallicity saturates in the inner disk lately, as seen in Fig. 6e).

In Figs. 7fgh it can be seen that colour gradients are established early on in the inner disk and propagate outwards. Extinction modifies slightly these profiles (especially the $B\text{--}K$ one), more at intermediate times than in the end of the evolution (for reasons explained in the previous paragraph). However, we find that extinction is not the main factor in shaping those gradients, in agreement with the analysis of Kuchinski et al. (1998) for the disks of spiral galaxies. The final colour profile presents an important gradient, extending up to 12-13 kpc. This is due to the fact that, inside that radius there are important differences in the star formation time-scales between e.g. 2-3 kpc and 6-7 kpc; inner regions have considerably older stellar populations than outer ones. However, outside the 12 kpc radius the disk is still young (star formation happens lately because of the long infall timescales) and colour gradients are not established.

The main point of this section concerns precisely the prediction of colour gradients in the inner disk, related to the existence of different scalelengths for the various wavelength bands. These features are a direct consequence of the inside-out formation scheme adopted here, on the basis of some theoretical arguments. A “uniform” formation of the disk (i.e. with the same timescale of star formation everywhere) would lead to similar scalelengths in all wavelengths and would create very small colour and metallicity gradients. On the other hand, extinction may certainly enhance colour gradients, but to a relatively small degree (at least with the prescriptions adopted in this work). The available data for the Milky Way allows only a very limited check of these ideas, but the large sample of observations concerning external spiral galaxies offers the opportunity for a detailed comparison; these issues are explored in a forthcoming paper (Boissier and Prantzos 1998).

3.3 Milky Way vs. solar neighborhood

In studies of the photometric (and, sometimes, chemical) evolution of spiral galaxies with one zone models, calibration is often made to the solar neighborhood observables, i.e. it

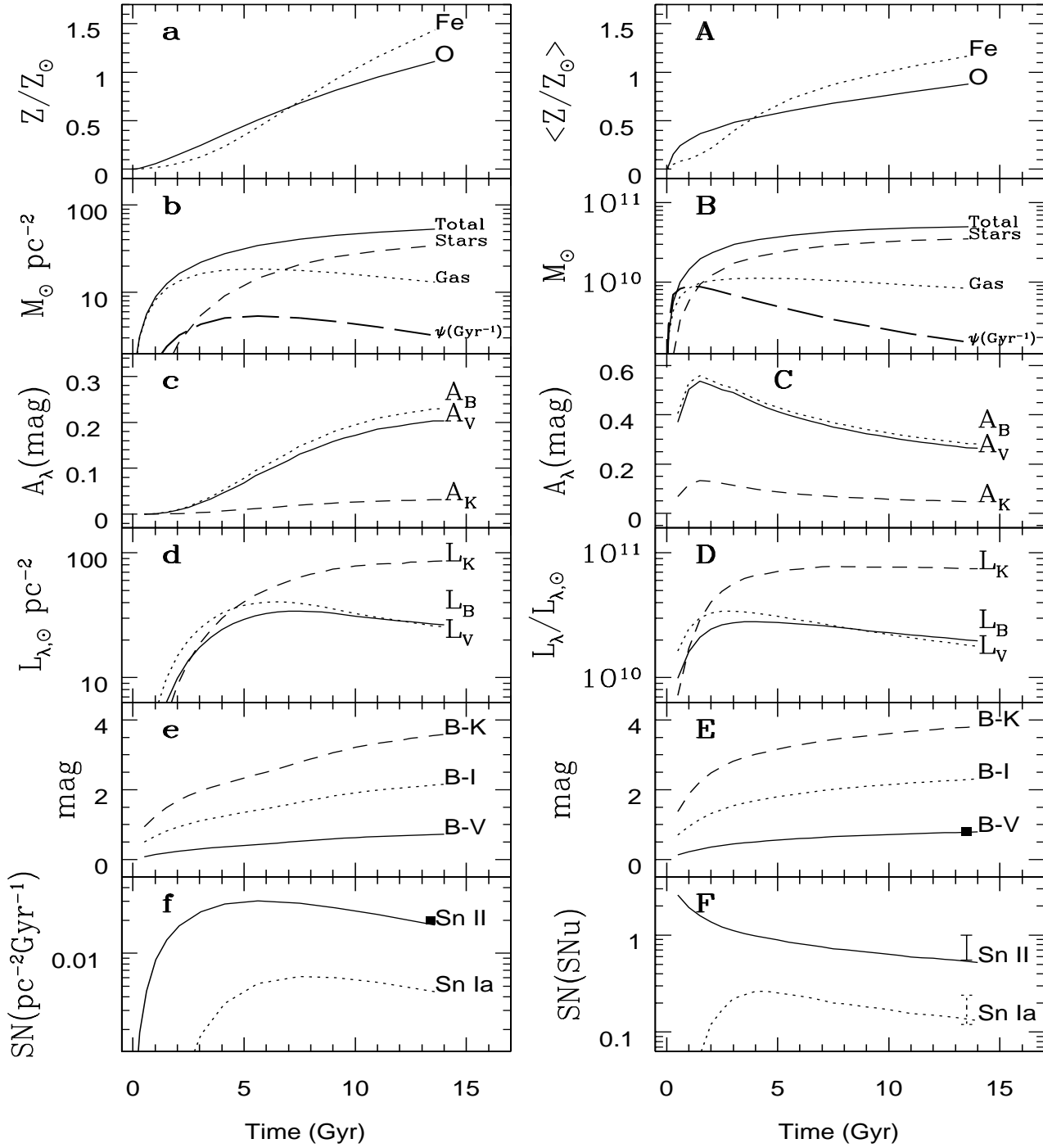


Figure 8. Comparison of the results for the chemo-photometric evolution of the solar neighborhood (on the left, see Sec. 3.1) and the one of the Milky Way (on the right, see Sec. 3.3 for the calculation of integrated or average properties). **a** and **A**: Evolution of Fe and O abundances on a linear scale; **b** and **B**: Evolution of gaseous, stellar and total mass (in $M_{\odot} \text{ pc}^{-2} \text{ Gyr}^{-1}$ on the left, in M_{\odot} on the right), as well as of star formation rate (corresponding units per Gyr); **c** and **C**: Evolution of extinction in the B -, V - and K - band; **d** and **D**: Evolution of B - (dotted), V - (solid) and K - (dashed) luminosities, with extinction included; **e** and **E**: Evolution of $B-K$, $B-I$ and $B-V$ colours (with extinction); **f** and **F**: Evolution of supernova rates; the local ones (Fig. 8f) are expressed in units of $\text{pc}^{-2} \text{ Gyr}^{-1}$, while the total ones (Fig. 8F) in SNU, i.e. the total SN rates (per century) are divided by the B - band luminosity, expressed in $10^{10} L_{B\odot}$. For observational data (filled squares or vertical error bars at $T=13.5$ Gyr) see Table 2 and references therein.

is assumed that the local disk evolution is representative of the average Milky Way disk evolution. In this section we check this assumption, in the framework of our model. We calculate total (extensive) quantities Q_T for the disk as:

$$Q_T(t) = \int_0^{R_G} 2 \pi q(R, t) R dR \quad (9)$$

where $q(R, t)$ is any quantity expressed in units of surface density (pc^{-2}) and R_G is the outer galactic radius. With this equation we obtain L_λ^0 when integrating the stellar luminosity alone, and L_λ when integrating the luminosity after correction for extinction at each radius. The “integrated” extinction is then $A_\lambda = -2.5 \log(L_\lambda/L_\lambda^0)$. Magnitudes and colours of the whole disk are computed from the integrated spectrum. We also calculate average (intensive) quantities as e.g. abundances. In this case, the average galactic value $< X_i >$ is

$$< X_i(t) > = \frac{\int_0^{R_G} 2 \pi X_i(R, t) \Sigma_{gas}(R, t) R dR}{\int_0^{R_G} 2 \pi \Sigma_{gas}(R, t) R dR} \quad (10)$$

The results are plotted in Fig. 8, where the solar neighborhood evolution (left part) is compared to the one of the Milky Way disk (right part). The final average Fe and O abundances in the gas of the disk (Fig. 8A) are similar to the ones in the solar neighborhood (Fig. 8a), but their history is different: early on, the average disk abundances are dominated by the inner galaxy which evolves more rapidly than the solar neighborhood; thus, the average disk metallicity increases more rapidly than the one of the local disk early on, whereas at late times the trend is inverted. The same behaviour is shown by the mass in stars and the SFR (Fig. 8b and 8B).

An issue of considerable interest is the one of the SFR vs. gas amount. In the case of the solar neighborhood, the current/maximum (q_{now}/q_{max}) ratio is ~ 0.7 for the gas surface density and ~ 0.5 for the SFR density (as expected from the $\Psi \propto \Sigma_G^{1.5}$ law adopted locally); both the gas and the SFR have a broad maximum around 5-6 Gyr. In the case of the Milky Way, the corresponding ratio is ~ 0.8 for the total gas and ~ 0.20 for the total SFR, i.e. those two global quantities do not obey the local Schmidt law; besides, their maxima do not coincide, being at ~ 3 -4 Gyr for the gas and ~ 1 -2 Gyr for the SFR. The reason of this behaviour is, of course, the non-linearity of the adopted SFR law, due both to the exponent (1.5) and the R^{-1} factor; both these factors enhance the SFR efficiency early on in the inner disk, where there is a lot of gas infalling rapidly. At late times, even if the total amount of gas is the same, it is distributed differently. A large part of the total SFR comes now from the outer regions (favoured by their larger area), where the SFR efficiency is small. In view of the importance of that topic, we make a more detailed analysis in Sec. 3.4, where a comparison to observational data of external spirals is performed.

In Fig. 8c and 8C it can be seen that there are also important differences between the Solar neighborhood and the Milky Way concerning the evolution of extinction. In the former case, A_B and A_V rise steadily, while in the latter they undergo an early maximum (due to the combined large amounts of gas and metals in the inner disk) and then decline steadily, since the gas in the inner regions is consumed and its metallicity barely increases; the outer regions play no role

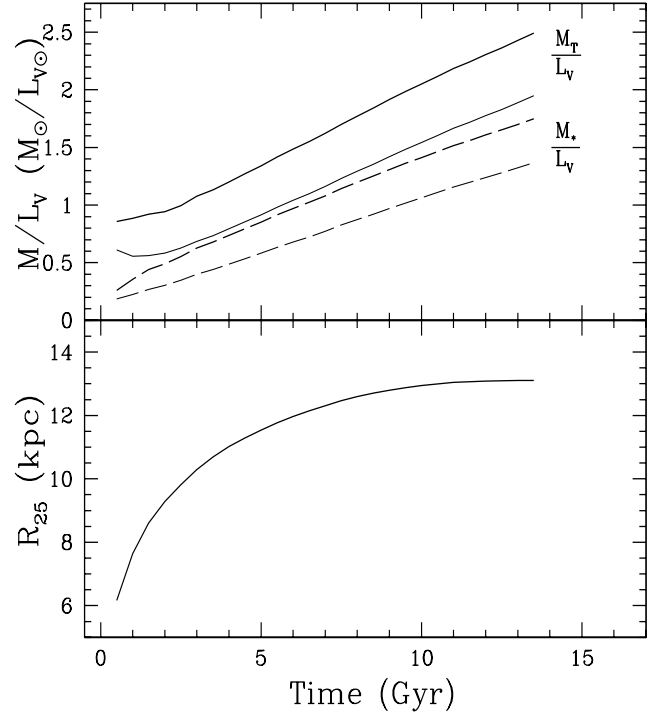


Figure 9. *Upper panel:* Evolution of the galactic M/L_V ratio for the total mass (solid curves) and the stellar mass (long dashed curves), with extinction neglected (i.e. stellar population alone, thin curves) or included (thick curves). *Lower panel:* Evolution of the isophotal radius R_{25} , at which the B -band surface brightness is equal to $25 \text{ mag arcsec}^{-2}$.

in the overall extinction, in view of their low column densities and metallicities.

The integrated luminosity of the Galaxy (Fig. 8D) evolves strongly in the first several Gyr, being dominated by the inner disk. After that period, the K -luminosity stays nearly constant (most of the galactic stars are already formed), while the B - and V - luminosities decrease slowly (because of the declining total SFR of Fig. 8B, although they do not follow it perfectly). At $R_S=8 \text{ kpc}$ (Fig 8d), luminosities rise and decline more slowly. This difference in time-scales is also present in the colour evolution (fig. 8e and 8E): while the solar neighborhood reddens steadily from $t=0$ to the present time, the integrated colours have an evolution which is more rapid at early times and slower at late times.

The SN rates for the whole disk (fig. 8F) are expressed in SNU (SN per century per $10^{10} L_{B\odot}$). The SNII frequency (in SNU) is high early on and decreases steadily, because L_B does not follow exactly the SFR (stars contributing to L_B are not as short lived as those exploding as SNII). The results at $T=13.5 \text{ Gyr}$ for both SNII and SNIa are closer to the rates reported (Tammann et al. 1994, Capellaro et al. 1997) for Sb rather than Sbc galaxies and for low rather than high values of the Hubble constant. (both factors, i.e. the Sb type and low Hubble value, lead to lower deduced frequencies in SNU).

Finally, the evolution of the M/L_V ratios, obtained by dividing the stellar and total mass of the disk (fig. 8B) by the L_V luminosity (fig. 8D), is shown in figure 9. Both quantities

increase steadily and more rapidly than in the case of the solar neighborhood (Fig. 5b), because most of the disk mass resides in the inner galaxy, which evolves more rapidly than the local disk. Also, the M/L_V ratio depends somewhat on the calculated amount of extinction (up to 45% in the early evolution and to 20% towards the end).

In summary, the overall evolution of the Milky Way disk bears little similarity to that of the solar neighborhood (or to any other region for that matter). Because of the non-linearity of the SFR efficiency with galactic radius, evolution is dominated by the inner disk at early times. At late times, most of the “action” takes place in the outer disk, which dominates extensive quantities (Equ. 9) that follow the SFR; at those late times, intensive quantities (Equ. 10) receive important contributions from the whole disk. This behaviour of spiral disks resulting from our model has important implications for the observations of external spirals, both at low and high redshift.

3.4 The average SFR in the Milky Way and normal spirals

The behaviour of local vs. global SFR, briefly discussed in the previous Section, is better illustrated in Fig. 10. The local SFR in each galactic zone obeys the adopted Schmidt law (upper pannel), but with considerably different efficiencies (because of the R^{-1} factor). However, the global SFR vs. total gas amount (middle pannel in Fig. 10) has a completely different behaviour: for the same gas amount, very different values of the SFR are found. It is true that the high values concern the early evolution (before the first 2 Gyr), where the SFR is dominated by the innermost regions of the disk and the adopted SFR prescription is probably not valid (since there are no spiral arms inside ~ 2 kpc, at least in the case of the current Milky Way). When the first 2 Gyr are neglected, we find a relationship between global SFR and gas amount (thick part of the curve in Fig. 10, middle), which corresponds to a slope of ~ 4 , i.e. $\text{SFR}_{\text{TOTAL}} \propto M_{\text{GAS}}^4$; this simply reflects the highly non-linear behaviour of the adopted SFR prescription, but *has no physical meaning* and cannot be used in any model of chemical evolution. Indeed, the important conclusion of this analysis is that, even if a Schmidt type SFR law is introduced locally, any radial dependence of the SFR efficiency will make the global SFR of a disk deviate considerably from this law. In other terms, *it is impossible to model spiral galaxies by one zone models with a fixed relationship between SFR and gas amount*. This would have some sense only if there were no radial variation in the SFR efficiency, but in that case *no gradients of abundances or colours would be obtained*, contrary to observational evidence.

A more physical insight is obtained by analysing the behaviour of *average* quantities, i.e. average SFR density vs. average gas density; both averages are made over some portion of the disk area. In a recent study concerning normal spiral galaxies and starbursts Kennicutt (1998) divides total SFR and Σ_{GAS} by $\pi R_{25}(B)^2$, where $R_{25}(B)$ is the radius at which the surface brightness in the B -band is equal to 25 mag arcsec $^{-2}$. The evolution of $R_{25}(B)$ in our model is given in Fig. 9 (lower pannel): it increases in the first 6 Gyr up to $R_{25} \sim 13.5$ kpc (because of the adopted infall and SFR laws) and stays roughly constant afterwards. By di-

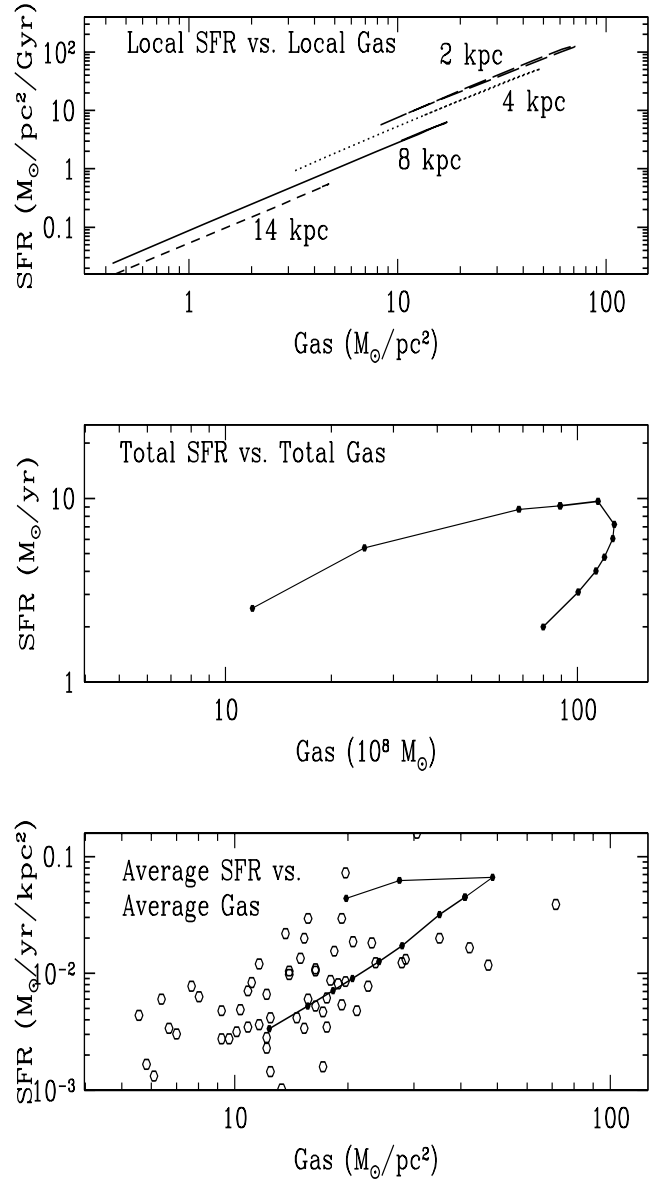


Figure 10. *Upper pannel:* Local relationship between SFR and gas surface densities for four zones of our model (curves) during the galactic evolution; for each zone, a unique Schmidt law with slope 1.5 is recovered, but the shift between the curves indicates that the R^{-1} factor increases the SFR efficiency in the inner regions. *Middle pannel:* Relationship between the total SFR and gas amount of the disk; evolution takes place from left to right in this diagram and points mark various instants in time (0.01, 0.1, 0.5, 1., 2., 4., 5.5, 7.5, 9., 11. and 13.5 Gyr, respectively). The local Schmidt law is not recovered globally, because of the non-linearity of the SFR across the disk (see the discussion in Sec. 3.3). *Lower pannel:* Relationship between the average SFR and average gas surface density in the disk; the quantities of the previous pannel are divided by πR_{25}^2 , where R_{25} is the radius at which $\mu_B = 25$ mag arcsec $^{-2}$. Results (solid curve with points marking several instants in time) are compared to observations in external spirals (open symbols); the data are from Kennicutt (1998), but the given amount of hydrogen ($\text{H}_2 + \text{HI}$) has been increased by 40%, to take He into account, as to be directly comparable with our results.

viding the model total SFR and Σ_{GAS} by $\pi R_{25}(B)^2$, we are able to compare directly our results to the data of Kennicutt (1998). His data for normal spirals are plotted also in Fig. 10 (lower pannel), but we increased his gas surface densities (concerning the sum of H_2+HI) by 40% ($=1./0.7$) to account for a contribution of 30% He by mass (to compare directly with our results). Our model curve (after the first 0.5 Gyr) lies well within the data points, i.e. the *absolute* values of the average SFR during the Milky Way evolution correspond fairly well to observations of external spirals. Also, after the first 0.5 Gyr we find a unique slope $N=1.7$ in the average SFR vs. gas surface density relationship. This value is to be compared with the values derived by Kennicutt (1998): $N=1.29\pm0.18$ for a conventional least squares fit to his data and $N=2.47\pm0.39$ for a bivariate least squares regression, taking into account uncertainties in both the SFR and the gas density. Kennicutt (1998) concludes that "...any Schmidt type law in these galaxies should be regarded as a very approximate parametrisation at best". We showed here that the adopted local Schmidt law leads to an average SFR compatible with available data for external spirals. However, this does not imply that the adopted $N=1.5$ is the real value of the local Schmidt law; our result only implies that, when combined with the R^{-1} factor for the SFR efficiency, the $N=1.5$ exponent leads to results that are compatible with all available observables in the Milky Way and with observations of the average SFR vs. gas density in other spirals. Some other combination (i.e. a different N and a different radial dependence of the SFR efficiency) could, perhaps, lead also to acceptable results.

4 CONCLUSIONS

We have developed a model computing coherently the chemical and spectrophotometric evolution of spiral disks. The model makes use of up-to-date input ingredients (i.e. stellar IMF and yields, metallicity dependent stellar lifetimes, evolutionary tracks and spectra) and considers the galactic disk as an ensemble of independently evolving concentric rings built by infall of gas of primordial composition. Its main ingredient is a radially dependent SFR ($\Psi(R) \propto \Sigma_G^{1.5} R^{-1}$), based both on empirical data (the $\Sigma_G^{1.5}$ part) and theoretical arguments (the R^{-1} part). In fact, we show here (Sec. 2.1.3 and Fig. 2) that the adopted SFR law, when applied to the gaseous profile of the Milky Way, gives results which compare fairly well with the observed SFR profile in our Galaxy. The model is then applied to the Milky Way evolution and the main results can be summarised as follows:

1) The main observational features of the Solar neighborhood and the Milky Way disk are fairly well reproduced, with the simple assumptions of a slow formation of the local disk (in timescales of many Gyr, in order to explain the observed local G-dwarf metallicity distribution) and a radial variation in the efficiency of star formation (to obtain the observed gas and abundance gradients).

2) The evolution of the abundance gradients is not really constrained by observations at present. In our model, abundance gradients are predicted to flatten with time and to finally saturate in the inner disk (in agreement with a few previous works on that topic). Also, the adopted prescription for the rate of SNIa (major Fe producers) reproduces suc-

cessfully a local observable (the decline of O/Fe with Fe/H in the solar neighborhood) and predicts a gradient of Fe/H steeper than the one of oxygen at all times (Sec. 3.2.1).

3) The predicted current SNII rate in the solar neighborhood is in fair agreement with observations ($2 \cdot 10^{-11}$ core collapse SN $pc^{-2} yr^{-1}$, Tamman et al. (1994)), showing that our choice of SFR and IMF are mutually consistent; this is also corroborated by the fact that the model reproduces fairly well the local Present Day Mass Function, something rarely considered in analogous studies (Sec. 3.1.1). More importantly, we obtain the total current rate of SNII and SNIa expressed in SNU, i.e. by calculating both the supernovae rates and the evolution of the blue luminosity of the Galaxy. The results are on the low range of (but compatible with) observations of external galaxies (Sec. 3.3 and Table 2).

4) We calculate the surface density profiles of the various stellar remnants (dominated always by white dwarfs). We find that currently in the solar neighborhood their contribution is smaller than the one of gas, while in the inner disk it is much larger and can reach $\sim 20\%$ of the stellar surface density (Sec. 3.2.1). We find that there should currently exist $\sim 10^{10}$ white dwarfs, $\sim 5 \cdot 10^8$ neutron stars and $\sim 5 \cdot 10^7$ black holes in the Galaxy (within a factor of ~ 2 , depending on the IMF and the mass of the disk). On the total, the galactic mass of compact objects is comparable to the one of gas, i.e. each contributes for $\sim 7-8 \cdot 10^9 M_\odot$ or $\sim 12-15\%$ of the mass of the disk. These results may have important implications for the statistics of microlensing events towards the bulge, or for the detection of galactic neutron stars and black holes in binary systems.

5) The use of metallicity dependent stellar tracks, lifetimes and spectra, along with a full chemical evolution model, is mandatory in studies of the photometric evolution of galaxies (especially of systems with large metallicity variations in long timescales, such as spirals, see Sec. 3.1.2). We also show that, when metallicity dependent lifetimes are used (as they should!) only the isochrone method is applicable when calculating the luminosity evolution of a galaxy (Sec. 2. 2).

6) The adopted scheme of star formation in the disk leads naturally to different scalelengths in the various photometric bands (shorter in the red and longer in the blue), in fair agreement with observations of the Milky Way disk for which we obtain: $H \sim 2.6$ kpc in the K band and $H \sim 4$ kpc in the B band (Sec. 3.2.2). Also, it produces galactic disks which are much more compact in the past, an important result in view of current studies of galaxy evolution at high redshifts.

7) For the same reason, colour gradients are obtained, first in the inner disk, then propagating outwards. We find no colour gradients in the outer disk, which is formed relatively late in that scheme, so that there is no time for colour gradients to be established there (Sec. 3.3.2). Moreover, we find that extinction enhances but does not really create colour gradients (at least with the adopted prescription).

8) The evolution of various parameters in the solar neighborhood (stars, gas, abundances, luminosities etc.) does not match the corresponding evolution (of average or global quantities) of the whole disk. This is due to the non-linearity of the adopted star formation law as a function of galactocentric radius. In particular, the early evolution of the Galaxy (dominated by the inner disk) is more rapid and

the late evolution slower than the one of the solar neighborhood. This implies that one-zone models reproducing the evolution of the solar neighborhood cannot be taken as representative of the evolution of the Milky Way as a whole (Sec. 3.3).

9) The adopted scheme of star formation (main ingredient of the model) compares fairly well to observations of average SFR vs. gas surface density of external spirals. Notice that such a comparison can be made only in the framework of chemo-photometric models since the R_{25} radius is required for the averaging (see Sec. 3.4)

We notice that the photometric results of our model depend strongly on the quality of the adopted stellar tracks and spectra. In that respect, the use of the now available homogeneous set of these ingredients presents a great improvement. However, the Geneva tracks include neither the Horizontal Branch (negligible in the context of this work) nor the thermally pulsing AGB phase (potentially more important, but certainly not able to invalidate our conclusions in points 6 and 7).

Finally, the success of the model does not necessarily imply its correctness. It suggests however that there may be a grain of truth in the overall picture, which should be further tested against a larger mass of observational data, concerning spiral galaxies at low and high redshifts. Work is in progress along these directions.

REFERENCES

- Allard F. & Hauschild P., 1995, ApJ, 445, 433
 Allen C., Carigi L. & Peimbert M., 1998, ApJ, 494, 247
 Anders E. & Grevesse N., 1989, *Geochimica and Cosmochimica Acta*, 53, 197
 Arimoto N., Yoshii Y. & Takahara F., 1992, A&A, 253, 21
 Baraffe I., Chabrier G., Allard F. & Hauschildt P., 1998, A&A 327, 1039
 Bazan G. & Mathews G., 1990, ApJ, 354, 64
 Bessell M., Brett J., Scholz M. & Wood P., 1991, A&AS, 89, 335
 Bethe H. & Brown G., 1995, ApJ, 445, L129
 Bethe H. & Brown G., 1998, *astro-ph/9805355*
 Boesgaard A.-M., King J., Deliyannis K. & Vogt S., 1999, AJ, 117, 492
 Bohlin R., Savage B. & Drake J., 1978, ApJ, 224, 132
 Bruzual A. & Charlot S., 1993, ApJ, 405, 538
 Calzetti D., Kinney A. & Storchi-Bergmann T., 1994, ApJ, 429, 582
 Capelarro E., Turatto M., Tsvetkov D., Bartunov O. Pollas C., Evans R. & Hamuy M., 1997, A&A, 322, 431
 Cardelli J. & Federman S., 1997, in *Nuclei in the Cosmos IV*, Eds. J. Gorres, G. Mathews, S. Shore & M. Wiecher (Elsevier), p. 31
 Carigi L., 1996, *Rev. Mexicana Astr. Astrofis.*, 32, 179
 Chamcham C. & Tayler R., 1994, MNRAS, 266, 282
 Charbonnel C., 1998, in *Abundance gradients as a diagnostic tool for galaxy evolution*, Eds. D. Friedly et al., ASP Conf. Series, p. 157
 Charbonnel C., Meynet G., Maeder A. & Schaerer D., 1996, A&AS, 115, 339
 Chiapini C., Matteucci F. & Gratton R., 1997, ApJ, 477, 765
 Clarke C., 1989, MNRAS, 238, 283
 Corradi R., Beckman J. & Simonneau E., 1996, MNRAS, 282, 1005
 Contardo G., Steinmetz M. & Fritze-von Alvensleben U., 1998, ApJ, 507, 497
 Coppi G., 1997, ApJ, 487, 704
 Cunha K. & Lambert D., 1994, ApJ, 426, 170
 Dame T., 1993, in *Back to the Galaxy*, Eds. S. Holt & F. Verter (AIP), p. 267
 Dopita M. & Ryder S., 1994, ApJ, 430, 163
 Dwek E., 1998, ApJ, 501, 643
 Edvardsson B., Andersson J., Gustafsson B., Lambert D., Nissen P. & Tomkin J., 1993, AA, 275, 101
 Ferrini F., Molla A., Pardi M. & Diaz A., 1994, ApJ, 427, 745
 Firmani C., Hernandez X. & Tutukov A., 1996, A&A, 403, 414
 Fluks M., Plez B., The P., De winter D., Westerlund B. & Steenman H., 1994, A&AS, 105, 311
 Francheschini A. et al., 1998, ApJ, 506, 600
 Freudenreich H., 1998, ApJ, 492, 495
 Gilmore G. & Wyse R. 1998, AJ, 176, 748
 Gilmore G., Wyse R. & Kuijken K., 1989, in *Evolutionary Phenomena in Galaxies*, Eds. J. Beckman & B. Pagel (Cambridge University press), p. 172
 Gilmore G., Parry I. & Ryan S., (Eds.) 1998, *The Stellar Initial Mass Function*, ym (San Francisco: ASP)
 Gizis J. & Reid I., 1999, AJ, in press
 Gould A., Bacall J. & Flynn C., 1997, ApJ, 482, 913
 Grevesse N., Noels A. & Sauval J., 1996, in *Cosmic Abundances*, Eds. S. Holt & G. Sonneborn (ASP Conf. Ser. 99), p. 13
 Guibert J., Lequeux J. & Viallefond F., 1978, A&A, 68, 1
 Guiderdoni B., Hivon E., Bouchet R. & Maffei B., 1998, MNRAS, 295, 877
 Guiderdoni B. & Rocca-Volmerange B., 1987, A&A, 186, 1
 Gummersbach C., Kaufer A., Schäffer D., Szeifert T. & Wolf B., 1998, A&A, 338, 881
 Gusten R. & Mezger M., 1983, *Vistas Astr.*, 26, 159
 Han C. & Chang K., 1998, MNRAS, 299, 1040
 Haywood M., 1994, A&A, 282, 444
 Iben I. & Tutukov A., 1984, ApJ, 284, 719
 Israelian G., Garcia-Lopez R. & Rebolo R., 1998, ApJ, 507, 805
 Jimenez R., Padoan P., Matteucci F., Heavens A., 1998, MNRAS, 299, 123
 Kennicutt R., 1989, ApJ, 344, 685
 Kennicutt R., 1998, ApJ, 498, 541
 Kent S., Dame T. & Fazio G., 1991, ApJ, 378, 131
 Köppen J., 1994, A&A, 281, 26
 Kroupa P., 1998, in *Brown Dwarfs and Extrasolar Planets*, Eds. R. Rebolo et al. (ASP Conf. 134), p. 483
 Kroupa P., Tout C. & Gilmore G., 1993, MNRAS, 262, 545
 Kulkarni S. & Heiles C., 1987, *Interstellar Processes*, Eds. D. Hollenbach & H. Thronson (Kluwer), p. 87
 Kuchinsky L., Terndrup D., Gordon K. & Witt A., 1998, *Astron. J.*, 115, 1438
 Kurucz R., 1995, CDROM
 Lacey C. & Fall M., 1986, ApJ, 290, 154
 Larson R., 1976, MNRAS, 176, 31
 Lejeune T., Cuisinier F. & Buser R., 1997, A&AS, 125, 229
 Lilly S. et al., 1998, ApJ, 500, 75
 Lyne A., Manchester R. & Taylor J., 1985, MNRAS, 213, 613
 Marigo P., Bressan A. & Chiosi C., 1996, A&A, 313, 545
 Massey P., Johnson K. & Degioia-Eastwood K., 1995, ApJ, 454, 151
 Massey P., 1998 in *Stellar astrophysics for the Local Group*, Eds E. Aparicio et al (Cambridge University Press), p. 95
 Mayor M. & Vigroux L., 1981, A&A, 98, 1
 Matteucci F. & Greggio L., 1986, A&A, 154, 279
 Mera D., Chabrier G. & Schaeffer R., 1998, A&A, 330, 953
 Molla M., Ferrini F. & Diaz A., 1997, ApJ, 475, 519
 Natta A. & Panagia N., 1984, ApJ, 287, 228
 Nomoto K., Iwamoto K. & Kishimoto N., 1997, *Science*, 276, 1378
 Onihishi T., 1975, *Progress in Theor. Phys.*, 53, 1042
 Pagel B., 1997, *Nucleosynthesis and Galactic Chemical Evolution*, CUP

- Prantzos N., 1994, A&A, 284, 477
 Prantzos N., 1996, A&A, 310, 106
 Prantzos N., 1998a, in *Primordial Nuclei and their Galactic Evolution*, Eds. N. Prantzos, M. Tosi & R. von Steiger (Kluwer) p. 225
 Prantzos N., 1998b, in *Abundance gradients as a diagnostic tool for galaxy evolution*, Eds. D. Friedly et al., ASP Conf. Series, p. 171
 Prantzos N. & Aubert O., 1995, A&A, 302, 69
 Prantzos N. & Silk J., 1998, ApJ, 507, 229
 Rana N., 1991, ARAA, 29, 129
 Renzini A. & Voli A., 1981, A&A, 94, 175
 Reid I.N. & J. Gizis, 1997, Astron. J., 113, 2246
 Robin A., 1998, private communication
 Robin A., Cr    M. & Mohan V., 1992, A&A, 265, 32
 Rocha-Pinto H. & Maciel W., 1996, MNRAS, 279, 447
 Rocha-Pinto H. & Maciel W., 1997, MNRAS, 325, 523
 Romani R., 1998, A&A, 333, 583
 Ruiz-Lapuente P. & Canal R., 1998, ApJ, 497, L57
 Ruphy S., Robin A., Epchtein N., Copet E., Bertin E., Fouque P. & Guglielmo F., A&A, 313, L21
 Sackett P., 1997, ApJ, 483, 103
 Salpeter E., 1955, ApJ, 121, 161
 Samland M., Hensler G. & Theis CH., 1997, ApJ, 476, 544
 Scalzo J., 1986, Fund. Cosm. Phys., 11, 1
 Scalzo J., 1998, [astro/ph-9811341](#)
 Schaller G., Schaerer D., Maeder A. & Meynet G., 1992, A&AS, 96, 269
 Shaver P., McGee R., Newton L., Danks A. & Pottasch S., 1983, MNRAS, 204, 53
 Smartt S. & Rolleston W., 1997, ApJ Let, 481, L47
 Steinmetz M. & Muller E., 1994, MNRAS, 276, 549
 Talbot R. Jr. & Arnett D., 1975, ApJ, 197, 551
 Tammann G., Loefer W. & Schroder A., 1994, ApJ Suppl., 92, 487
 Thielemann K.-F., Nomoto K. & Yokoi K., 1986, A&A, 158, 17
 Thielemann K.-F., Nomoto K. & Hashimoto M., 1996, ApJ, 460, 408
 Thomas D., Greggio L. & Bender R., 1998, MNRAS, 296, 119
 Thorsett S. & Chakrabarty D. 1998, ApJ, submitted
 Timmes F., Woosley S. & Weaver T., 1995, ApJ Suppl., 98, 617
 Timmes F., Woosley S. & Weaver T., 1996, ApJ, 457, 834
 Tinsley B., 1980, Fund. Cosm. Phys., 5, 287
 Tosi M., 1988, A&A, 197, 33
 Tosi M., 1998, in *Primordial Nuclei and their Galactic Evolution*, Eds. N. Prantzos, M. Tosi & R. von Steiger (Kluwer) p. 207
 Tsujimoto T., Yoshii Y., Nomoto K. & Shigeyama T., 1995, A&A, 302, 704
 van der Kruit P., 1986, A&A, 157, 230
 Vilchez J. & Esteban C., 1996, MNRAS, 280, 720
 Wang Z., 1990, ApJ, 360, 529
 Wang B. & Silk, J. 1994, ApJ, 427, 759
 Woosley S. & Weaver T., 1995, ApJ Suppl., 101, 181
 Wyse R. & Gilmore G., 1995, AJ, 110, 2771
 Wyse, R. & Silk, J. 1989, ApJ, 339, 700
 Xu C., Buat V., Boselli A. & Gavazzi G., 1997, A&A, 324,32